Review of Terramechanics Models and Their Applicability to Real-time Applications

Rui He[a], Corina Sandu [a], Aamir K. Khan[a], A. Glenn Guthrie[b], P. Schalk Els [b] and Herman A. Hamersma[b]

[a] Terramechanics, Multibody, and Vehicle Systems (TMVS) Laboratory, Department of Mechanical Engineering, Virginia Polytechnic Institute and State University, Blacksburg, VA 24061, United States. herui33@vt.edu, aamirk@vt.edu, csandu@vt.edu

[b] Vehicle Dynamics Group (VDG), Department of Mechanical and Aeronautical Engineering, University of Pretoria, Pretoria, 0002, South Africa. glenn.guth@gmail.com, Schalk.Els@up.ac.za, hermanh@up.ac.za

Abstract

ISTVS embarked on a project in 2016 that aims at updating the current ISTVS standards related to nomenclature, definitions, and measurement techniques for modelling, parameterizing, and, respectively, testing and validation of soft soil parameters and vehicle running gear-terrain interaction. As part of this project, a comprehensive literature review was conducted on the parameterization of fundamental terramechanics models. Soil parameters of the empirical models to assess off-road vehicle mobility, and parameters of the models to characterize the response of the terrain interacting with running gears or plates from the existing terramechanics literature and other researchers' reports were identified. This review documents and summarizes the modelling approaches that may be applicable to real-time applications of terramechanics in simulation, as well as in controller design.

Keywords: Soil modeling; Pressure-sinkage models; Shear stress-displacement models; Vibration models; ISTVS standards; Terramechanics; Off-road vehicle dynamics

1. Introduction

Modelling terrain-vehicle and terrain-machinery interaction has been the mission of the International Society of Terrain-Vehicle Systems (ISTVS) since its inception in 1962. Off-road vehicles, earthmoving and construction equipment, and agricultural and forestry machinery remain vital to the global economy. In 2016, the ISTVS embarked on a project to update the existing ISTVS standards in an attempt to bring standardization and conformity to the community working in the field of terramechanics. Additionally, many real-time applications of Terramechanics and

off-road vehicle dynamics have emerged over the past two decades. This presents an opportunity to improve the measurement and control of off-road vehicles and machinery. The two main application fields are real-time dynamic simulation and real-time controller design.

An extensive literature review was performed as part of the ISTVS standards initiative. This paper reports specifically on the aspects of this literature review that could be potentially valuable for real-time applications, including:

a) Pressure sinkage models for zero slip (applicable to non-driven and non-steered wheels)
b) Pressure sinkage models for non-zero slip (applicable to driven and/or steered wheels)
c) Shear stress – shear displacement models (traction / braking)
d) Running gear-terrain or plate-terrain vibration models

For real-time controller design and implementation, the focus is on states, parameters and properties that

a) are known beforehand (as in rover applications where moisture content may be known, e.g. dry lunar dust)
b) can be directly measured in real time e.g. wheel slip, rut depth, slip angle, etc. (Botha and Els, 2015a), (Botha and Els, 2015b), (Johnson et al., 2017)
c) can be "previewed" or obtained from a detailed terrain map (e.g. terrain profile, slope etc.) or from wheelbase preview where events on the front wheel of a vehicle can be used to predict or estimate what will happen on the 2nd, 3rd etc. wheels in the same rut or track (Linström et al., 2018)
d) can be estimated using easily measureable vehicle states (e.g. mass, center of mass position etc.) (Sandu et al., 2015)

This work, therefore, includes a thorough review of the literature to demonstrate which soil parameters, modelling techniques, experimental methodologies and equipment have been used or are currently being used by the community with a view to standardizing experimental procedures for measurement of soil parameters and parameterization of terramechanics models. Lack of standardization is currently an obstacle in terramechanics research because different equipment and methodologies make comparison of results between different studies extremely difficult.

Section 2 discusses some work done towards implementing terramechanics modeling in real-time and some of the challenges experienced in the real-time environment. Section 3 describes the most common soil paramters of empirical off-road vehicle mobility models. Section 4 discusses modelling terrain response to vehicle loading and describes the

equipment and methodologies used to parameterize these models. Section 5 introduces some emerging measurement techniques that hold potential for real-time application in the terramechanics community.

The approach can be summarized as: i) the soil paramters of terramehcanics models are extracted and listed besides introducations of the models; ii) the information about the parameterization of terramehcanics models from the previous literature is gathered and tabulated with the test soil and experimental methodology listed. Although terramechanics model parameters include soil parameteres, vehicle parameters, etc., only soil parameters are discussed herein. In the interest of space, only fundamental models about terrain response, plate-terrain interaction, and running gear-terrain interaction which the authors of this paper think have been reasonably parameterized are investigated herein. Models that are derived based on those fundamentals, e.g., multiple models reviewed by Taheri et al (Taheri et al., 2015), or without rigorous parameterization are not included in this work.

2. Existing terramechanics research in the real-time environment

Madsen et al. applied parallel computing techniques and incorporated soil mechanics theoretical models (Boussinesq equation, Cerruti equation, and bulldozing force equation) and an empirical shear stress-displacement model into the real-time simulation of vehicle running on soft soil (Madsen et al., 2012) . The Boussinesq equation and the Cerruti equation were used to compute the soil vertical stress induced by vertical and horizontal forces respectively. The bulldozing force equation and Janosi and Hanamoto empirical shear stress-displacement equation were utilized to calculate the tire force. Apart from the simulation of flexible tire-soil interaction when a vehicle traverses soft soil, the real-time simulation of a planetary rover over deformable terrain performed in the Rover Analysis, Modeling and Simulation (ROAMS) system also applied fundamental soil mechanics models such as the equation of the Mohr-Coulomb failure criterion (Jain et al., 2004).

Experimental tests on a wheel rolling over planetary Regolith Simulant in a single wheel test bed were used to parameterize a tire-soil traction model (Yoshida et al., 2006). Data from the tests was used to create plots of drawbar pull vs. slip ratio to identify the traction margin and slip. This traction model was used in a real-time traction controller to calculate drawbar pull and slope climbing capability for planetary rovers.

Another example of using data from experimental tests in off-road conditions for traction controller design is, Savitski et al. conducted tire-ice traction tests at various levels of tire normal load and created a database using the test data for the real-time traction control of a sport utility vehicle on an icy road (Savitski et al., 2017).

It is evident from these real-time applications that some fundamental terramechanics models, fundamental soil mechanics models, and experimental tests in off-road conditions play important roles in those applications. When using the fundamental terramechanics and soil mechanics models, model parameterization is an essential requirement. Parameterization inevitably requires appropriate experimental tests in off-road conditions if the employed model aims to accurately capture physics. Selection of appropriate test equipment, soil parameters and measurement methods result in effective experimental tests under off-road conditions, Furthermore, proper arrangements of experimental tests contribute to an effective parameterization methodology for a model.

3. Soil parameters required for empirical off-road vehicle mobility models

The empirical models to assess off-road vehicle mobility (OVM) establish relationships between the model outputs and model inputs purely based on experimental data. The model output can be some of the vehicle mobility parameters such as drawbar pull coefficient, motion resistance, drawbar pull efficiency, etc. The model inputs include vehicle parameters and soil parameters. The most typical soil parameters of the OVM empirical models available in literature are summarized in Table 1. Due to the large number of the OVM empirical models that have been proposed in the past, and because of this paper's topic focusing on soil parameters, formulas and other details of the cited OVM empirical models are not presented here, and readers interested in the formulas and more details should consult the references listed, or papers with comprehensive review on OVM empirical models (M. I. Lyasko, 2010), (M. Lyasko, 2010a), (Taheri et al., 2015), (Tiwari et al., 2010).

Table 1 Summary of soil parameters for empirical models to assess off-road vehicle mobility.

Soil Parameters	**Example Use of the Soil Parameter in OVM Empirical Model**	**References**
Cone index (CI)	Tire-clay numeric to correlate with drawbar coefficient	(Freitag, 1966)
Sand penetration resistance gradient	Tire-sand numeric to correlate with drawbar coefficient	(Turnage, 1972)
Remolding index (RI)	Towed motion resistance coefficient, net maximum drawbar pull coefficient	(Rula and Nuttall, 1971)
Rating cone index (RCI)		
Natural cover (roots),	Net traction ratio, rolling resistance ratio	(Schreiber and Kutzbach,

Upper soil strength, Lower soil strength, Clay content, Soil moisture content		2008)
Penetration resistance (pressure) Gravimetric water content Soil slope	Draught (drawbar pull if there is no plough), travel speed	(Boon et al., 2005)
Soil cohesion Soil friction angle	Mobility number to correlate with the lateral force ratio	(Gee-Clough and Sommer, 1981)

Compared with soil physical property parameters such as bulk density and water content, and soil mechanics parameters such as soil cohesion and soil friction angle, soil parameters such as Cone Index (CI), Remolding Index (RI), Rating Cone Index (RCI), and penetration resistance gradient which can be evaluated or measured by cone penetrometer are more commonly used in OVM empirical models (M. I. Lyasko, 2010). Mentioned yet not defined in the ISTVS 1977 standards, the cone index (CI), or sometimes referred to as the cone penetration resistance (pressure), was defined by the ASABE Standards (ASAE, 1999) as the force per unit base area required to push the cone penetrometer through a specified small increment of soil. The cone index (CI) serves as the soil parameter in many OVM empirical models, an example is an OVM empirical model specifically for clay that correlates a tire performance parameter such as drawbar coefficient or drawbar efficiency at certain slip ratio to a dimensionless soil-tire numeric, the clay-tire numeric (Freitag, 1966). For purely frictional terrain such as sand, the soil-tire numeric is the tire-sand numeric which uses the sand penetration resistance gradient instead of CI as the soil parameter. (Rula and Nuttall, 1971), (Turnage, 1974). The RI (Sloss, 1977) is defined as the ratio of the remolding soil strength to the original strength. The RCI is simply the product of the CI and the RI and it assesses the soil strength for the soil subjected to repeated traffic. For fine-grained soils, traction performance parameters can be modelled empirically as the function of the difference between RCI and a vehicle parameter called the vehicle cone index (Rula and Nuttall, 1971).

Although use of CI-related soil parameters can be largely seen in development of OVM empirical models, the CI – related soil parameters alone cannot fully characterize the soil strength, as water content and bulk density can also influence the soil strength (M. I. Lyasko, 2010), (Ayers and Perumpral, 1982). Gee-Clough and Sommer doubted the validity of CI to characterize the soil strength in OVM empirical model, and came up with new mobility numbers that

used traditional soil mechanics parameters such as soil cohesion and soil friction angle. These new mobility numbers were used to be the model inputs of the empirical models to compute wheel steering forces (Gee-Clough and Sommer, 1981). Schreiber and Kutzbach modelled the net traction ratio and rolling resistance ratio as empirical functions of tire parameters and soil parameters such as natural cover, upper soil strength, lower soil strength, clay content, and soil moisture content (Schreiber and Kutzbach, 2008). Other than the clay content and the soil moisture content which are common soil physical property parameters, the rest of the soil parameters were not defined, and how to determine them experimentally was no explained by Schreiber and Kutzbach, though their sample values were given (Schreiber and Kutzbach, 2008). Spatial maps of tractor travel speed, terrain slope gradiant, wheel slip, wheel torque, draught, penetration resistance and moisture content were measured and plotted (Boon et al., 2005). Based on these maps, Boon et al. empirically modelled travel speed as a function of wheel slip, wheel torque and terrain slope gradient, and draught as a function of travel speed, penetration resistance, and moisture content (Boon et al., 2005).

As can be seen from Table 1, parameterization of the OVM emprical models listed requires measurements of some soil physical property parameters, soil mechanics parameters, and CI-related soil parameters. The authors of this paper think these soil parameters are difficult, impractical or impossible to measure during real-time vehicle operation but together with the OVM empirical models have value during the development stages of vehicles and controllers (Vantsevich et al., 2017).

4. Modelling terrain response

The characterization of soil response to various loading scenarios is one of the primary interests of the terramechanics community. There are many models available to characterize the terrain response using different approaches, and depending on the approach, these models can be divided into three categories:

1. theoretical models, i.e., models derived from theory of mechanics or theory of other branches of physics, experimental results are used to validate not to derive these models;
2. empirical models, i.e., models derived from experimental results, and other experimental results are need to validate these models; and
3. semi-empirical models, i.e., the derivation of these models are based on combination of experimental results and theories of physics.

Some of these models are valuable not only because they can accurately depict terrain behavior under specific loading, but also because they are able to be conveniently incorporated into the chosen methodologies to study off-road vehicle or running gear performance or because they provide the basis to develop a more complex, higher fidelity model. Examples of more complex, higher fidelity models are the finite element model or the hybrid model to characterize the tire-terrain interaction (Taheri et al., 2015). This section details the models available in the literature and list the equipment and tests required to parameterize them.

4.1 Pressure-sinkage models

In the ISTVS 1977 standards, sinkage was defined as the distance from the lowest point on the track or wheel (the running gear) to the undisturbed soil or snow surface, measured normal to the surface (Sloss, 1977). In this article, what was defined in the ISTVS 1977 standards is named sinkage of some running gear (e.g., sinkage of wheel, sinkage of tire, etc.) and the term sinkage only means the sinkage of terrain, a type of terrain response, which is in agreement with the sinkage defined by Wong (Wong, 2008).

Pressure-sinkage models seek to quantify the amount of sinkage experienced when soil is subjected to a specific pressure from some pressure source. The pressure source can be a circular plate, rectangular plate, or a certain running gear, such as a wheel or tire. The sinkage due to the normal load of the pressure source is named static sinkage (Ishigami, 2008). The sinkage due to the slip between the pressure source and terrain is named slip sinkage, unlike some planetary rover wheel research in which such sinkage was named dynamic sinkage (Ishigami, 2008). When slip doesn't occur between the pressure source and the terrain, and the vertical acceleration of the pressure source is negligible, the sinkage can be assumed to be purely static sinkage. When slip occurs, the sinkage is considered to be made up of two components, one is static sinkage, and the other is slip sinkage (Reece, 1965), (Ishigami, 2008). This section divides the pressure-sinkage models into two groups, the models for zero slip, and the models for non-zero slip, and give introductions about them respectively.

4.1.1 Pressure-sinkage models for zero slip

Multiple efforts have been made to develop empirical models that characterize the pressure-sinkage relationship. Assuming that the soil to be modelled from the surface to the depth of interest is homogeneous, Bernstein proposed an

empirical model that has possibly the simplest form to characterize the pressure-sinkage relationship for plate-soil interaction (Bernstein, 1913):

$$p = kz^n \tag{1}$$

where p is the pressure applied to the soil, z is the sinkage of soil, and the sinkage modulus k and the sinkage exponent n are model parameters.

Later, the Bernstein model was modified for soil under a circular plate of diameter D such that the sinkage modulus would have a specific dimension, as shown in Eq. (2) (Saakyan, 1959). This model indicates that when the sinkage is small as the circular plate comes into contact with the soil, the rate of pressure increase could be very large. Kacigin and Guskovt confirmed this with experimental results of a plate-sinkage test (Kacigin and Guskovt, 1968).

$$p = k\left(\frac{z}{D}\right)^n \tag{2}$$

Bekker separated the sinkage modulus of the Bernstein model into two parts, one represents the effect of soil cohesion, and the other represents the effect of the angle of internal shearing resistance. Also, the geometry of the contact patch was taken into account by the Bekker model, as shown below (Bekker, 1969):

$$p = \left(\frac{k_c}{b} + k_\phi\right) z^n \tag{3}$$

where b is the smaller dimension of the contact patch, k_c is a sinkage modulus influenced by soil cohesion, and k_ϕ is a sinkage modulus influenced by soil friction angle.

Inspired by the approach adopted by Osman (Osman, 1964) and Meyerhof (Meyerhof, 1951) to study the failure pattern of the soil under a long flat plate, Reece developed two pressure-sinkage models (Eqs. (4) and (5)) where Eq. (5) was developed for very compact soils (Reece, 1965), (Onafeko and Reece, 1967). Unlike the Bekker model, the model parameters of Eq. (5) are dimensionless, and the dimension of the model parameters of Eqs. (4) is independent from the value of the sinkage exponent:

$$p = \left(k_1 + k_2 b\right)\left(\frac{z}{b}\right)^n \tag{4}$$

where k_1 and k_2 are model parameters,

$$p = \left(ck_c + \gamma k_\phi b\right)\left(\frac{z}{b}\right)^n \tag{5}$$

where c is the soil cohension, and γ is the unit weight of the soil.

Later, by combining the bearing capacity models proposed by Terzaghi and Housel, and the Bekker or Reece pressure-sinkage model, a new pressure-sinkage model for plate-soil interaction was found by Youssef and Ali (Youssef and Ali, 1982):

$$p = \left(K_1 + \alpha b K_2\right)\left(\beta\right)^n \left(\frac{z}{b}\right)^n \tag{6}$$

where K_1 and K_2 are soil shear strength values, and α and β are dimensionless geometric constants.

These aforementioned pressure-sinkage models are valid only for one type of pressure source, namely a plate pressing vertically (in the global coordinate system) against the soil (no lateral or longitudinal motion) such that the pressure in the plate-soil interface is vertical. For a wheel interacting with soil, the soil is also compressed in the radial direction. Assuming that the radial stress acting on the wheel rim is equal to the normal pressure beneath a plate at the same depth, and that the radial stress distribution is symmetric w.r.t. the radius that passes the maximum radial stress point, the Reece pressure-sinkage model was modified to characterize the radial stress along the wheel-soil interface (Wong and Reece, 1967a), (Wong and Reece, 1967b):

$$p(\theta) = \begin{cases} \left(k_1 + k_2 b\right)\left(\frac{r}{b}\right)^n \left(\cos\theta - \cos\theta_1\right)^n & \left(\theta_M \le \theta < \theta_1\right) \\ \left(k_1 + k_2 b\right)\left(\frac{r}{b}\right)^n \left\{\cos\left[\theta_1 - \left(\frac{\theta - \theta_2}{\theta_M - \theta_2}\right)\left(\theta_1 - \theta_M\right)\right] - \cos\theta_1\right\}^n & \left(\theta_2 < \theta \le \theta_M\right) \end{cases} \tag{7}$$

where θ is an arbitrary wheel angle, θ_1 is the entry angle (the acute angle between the centerline of the wheel and the beginning of contact), θ_2 is the exit angle (the acute angle between the centerline of the wheel and the end of contact), θ_M is the maximum radial stress point, and r is the radius of the wheel.

Noticing the dependence of pressure-sinkage relationship upon the test wheel diameter, a pressure-sinkage model specifically for the wheel-soil interaction was developed by Meirion-Griffith and Spenko (Meirion-Griffith and Spenko, 2011):

$$p = \hat{k} z^{\hat{n}} D^{\hat{m}} \tag{8}$$

where D is the diameter of the wheel, and $\hat{k}$, $\hat{n}$ and $\hat{m}$ are model parameters.

Later, the model was modified with the wheel width included for small-diameter wheel on compacted soil (Meirion-Griffith and Spenko, 2013):

$$p = \hat{k} z^{\hat{n}} \left(bl\right)^{\hat{m}} \tag{9}$$

$$l = \sqrt{D z_0 - z_0^2} \tag{10}$$

where b is the wheel width, l is the horizontally projected length of the wheel-soil contact patch, and z_0 is the maximum wheel sinkage.

All these empirical pressure-sinkage models introduced so far share one common feature namely that the sinkage z has a sinkage exponent n. There are other empirical pressure-sinkage models without this feature that include an exponential function of the sinkage z. Korchunov studied the pressure-relationship of moist soil that had low bearing capacity and proved theoretically and experimentally the following model predicted sinkage in good agreement with the experiment data (Korchunov, 1948), (Kacigin and Guskovt, 1968):

$$p = p_0 \left[1 - \exp\left(-z / k_0\right)\right] \tag{11}$$

$$p_0 = A_0 + B_0 \frac{M}{S} \tag{12}$$

where k_0 is the deformation constant with the same unit as that of the sinkage z, p_0 is the bearing capacity for plates of different sizes, A_0 is the maximum compressive stress, B_0 is the maximum resistance along the plate perimeter, M is the perimeter of the plate, and S is the area of the plate.

Later, Evans proposed an empirical pressure-sinkage model with similar form to that of the Korchunov model specifically for track-clay interaction. (Evans, 1953) (Plackett, 1985):

$$p = 8.28c\left(1 - \exp\left(-K\, z/b\right)\right) \tag{13}$$

where c is the clay cohesion, b is the track width, and K is an empirical model parameter.

Almost in the same era when the Bekker model was proposed, Kacigin and Guskovt established a semi-empricial hyperbolic law to characterize pressure-sinkage relationship of soil based on the experimental pressure-sinkage curve

(Kacigin and Guskovt, 1968). The derivation of the model took into account the feature of the pressure-sinkage curve at small sinkage, which could be represented by a linear function, and the feature of the pressure-sinkage curve at large sinkage where the pressure approaches an asymptote that represents the bearing capacity of the soil:

$$p = p_0 \frac{1-\exp\left(-2kz/p_0\right)}{1+\exp\left(-2kz/p_0\right)} \quad (14)$$

where p_0 is the bearing capacity of the soil, and k is the coefficient of volumetric compression.

Gottenland and Bonoit proposed an empirical sinkage-pressure model for circular plate-soil interaction (Gotteland and Benoit, 2006). The model is a product of one linear function of the sinkage z and another compound function that includes an exponential function of the sinkage z. The first linear function captures the linear sinkage-pressure relationship for both the elastic zone and the plastic zone of the sinkage-pressure plot. The transition from the elastic zone to the plastic zone is characterized by the second compound function with the exponential term. The model features two different asymptotes for the elastic zone and the plastic zone respectively, which disassociates the elastic and plastic behaviors of the soil:

$$p = \left(\frac{C_m}{B^m} + \frac{s_m}{B^{1-m}} z\right)\left(1-\exp\left\{-\frac{s_0}{C_m}\frac{z}{B^{1-m}}\right\}\right) \quad (15)$$

where B is the plate diameter, and C_m, s_0, s_m and m are the model parameters.

For the same soil but different plates or running gears, the classical empirical pressure-sinkage models, such as the Bekker model and the Reece model, will have a constant sinkage exponent and a varying sinkage modulus. By setting a constant sinkage modulus and the remaining part as a function of plate or running gear parameters and motion state parameters, Ding el al. developed a model (the Ding et al. 2014 model) that can reflect the influence of normal load, plate or running gear dimension, or slip in pressure-sinkage relationship (Ding et al., 2014). The general form of Ding et al. 2014 model is:

$$p = K_s z \lambda_N \quad (16)$$

where K_s is the sinkage modulus of the terrain in units of Pa/m, and λ_N is a dimensionless function of plate or running gear parameters such as the radius and width, and of motion state parameters such as the sinkage, normal load and slip.

The expression of the dimensionless function depends on the soil type and the experimental pressure-sinkage data, and plays a key role in accuracy of this model. For the soils with their Bekker model parameters listed by (Wong, 2008), their dimensionless function can be given by Eq. (17) if the soils have sinkage exponents larger than 0.3.

$$\lambda_N = \left(\frac{z}{z_0} \right)^{n_0 - 1 + n_1 (z/z_0)} \tag{17}$$

where $z_0 = 1\text{m}$, and n_0 and n_1 are the function parameters.

If the soils have sinkage exponents smaller than 0.3, which means the plastic phase of the pressure-sinkage relationship already begins at small sinkage, their dimensionless function can be written as:

$$\lambda_N = \frac{1}{n_0 + n_1 (z/z_0) + n_2 (z/z_0)^2} \tag{18}$$

where n_0, n_1 and n_2 are the function parameters.

In cases of small normal load less than 300 N and circular plates with radii from 25 mm to 50 mm, the running gear dimension effect was characterized by the dimensionless function:

$$\lambda_N = \left(\frac{z}{z_0} \right)^{n_0 - 1 + n_1 r} \tag{19}$$

where r is the radius of the circulate plate.

In cases of normal loads smaller than 7000 N and circular plates with radii ranging from 25.4 mm to 152.4 mm, the plate dimension effect can be characterized by:

$$\lambda_N = \left(\frac{z}{z_0} \right)^{n_0 - 1 + n_1 r + n_2 r^2} \tag{20}$$

However, Ding et al., made an observation that the model accuracy could be improved for such cases by setting the dimensionless function as an explicit function of the normal load, as shown below. By doing so, the plate dimension effect is implicitly considered as the values of function parameters n_0, n_1 and n_2 differ between two plates of different dimensions.

$$\lambda_N = \left(\frac{z}{z_0} \right)^{n_0 - 1 + n_1 W + n_2 W^2} \tag{21}$$

where W is the normal load applied to the soil by the plate.

There is, however, a concern regarding the influence of normal load on the pressure-sinkage relationship as described in (Ding et al., 2014). By replacing the normal load as the product of the plate area and pressure (Ding et al., 2014) in Eq. (21), and substituting the Eq. (21) to the general form of Ding et al. 2014 model, one end up with Eq. (22):

$$p = f\left(z, p\right) \tag{22}$$

Eq.(22) is an implicit function. Solving this implicit equation, the pressure will be represented as a new explicit function of sinkage z, which has a different form from that of the Ding et al. 2014 model. The new explicit function will show no influence of the normal load.

In cases of large normal loads smaller than 12000 N and rectangular plates with 457mm length and widths ranging from 12.5 to 101.6mm, the dimensionless function is similar to that in the cases of large normal load and circular plate as described above, with the only difference being that the radius is replaced by the width of the rectangular plate. Also, for cases of large normal load and rectangular plates, model accuracy could be improved by setting the normal load instead of plate width as the explicit variable of the dimensionless function (Ding et al., 2014).

In an in-situ steering test (Ding et al., 2017), a steering moment was applied to a wheel that had been previously in static equilibrium, then the wheel started to rotate about its vertical axis at a constant yaw rate. Ding el al. observed that during the steering test, sinkage increased with steering angle. This is because the steering produces soil flow, while in static equilibrium, there is no soil flow. When steering happens to the wheel previously in static equilibrium, sinkage will consist of static sinkage due to the wheel normal load plus an additional sinkage (steering sinkage) due to the steering. The Bekker model was modified by Ding et al. to take the steering sinkage into account:

$$p = \left(\frac{k_c}{b} + k_\phi\right) z^{N_s(\theta_s, W)} \tag{23}$$

$$N_s(\theta_s, W) = n_0 + n_1 \theta_s^{\alpha_1 + \beta_1 W} \tag{24}$$

where N_s is the sinkage exponent as a function of steering angle θ_s and the normal load of the wheel W, and n_0, n_1, and α_1, and β_1 are the model parameter of the sinkage exponent model.

Pressure-sinkage models have also been proposed for organic terrain (unless specified to be organic terrain, all the terrains that appear in this paper are non-organic terrain). Assuming that the organic terrain (muskeg) is made up of two

layers, the surface mat and the peat, Wong et al. came up with an empirical pressure-sinkage model for the muskeg (Wong et al., 1982):

$$p = k_p z + 4 m_m z^2 / D_h \text{ if } z \le z_{cr} \quad (25)$$

$$D_h = 4A/L \quad (26)$$

where k_p is the stiffness parameter for the peat, m_m is the strength parameter for the surface mat, D_h is the hydraulic diameter of the contact patch, z_{cr} is the critical sinkage where breaking of the surface mat starts, A is the area of the contact patch, and L is the perimeter of the contact patch.

For vehicles with multiple axles, where the wheels follow the same ruts, apply multiple loading-unloading-reloading cycles are applied to the soil. Wong et al. developed Eqs. (27) and (28) to characterize the pressure-sinkage relationship for the unloading-reloading cycle (Wong et al., 1984):

$$p = p_u - k_u (z_u - z) \quad (27)$$

$$k_u = k_0 + A_u z_u \quad (28)$$

where p_u and z_u are the pressure and sinkage, respectively, when unloading starts, k_u is the average slope of the unloading-reloading line on the pressure-sinkage plot, and k_0 and A_u are model parameters.

In classical soil mechanics, for studies of foundation and settlement, the following empirical model that links soil sinkage, normal load and plate-soil contact patch can be used (Tsytovich, 1963):

$$z = Tp\sqrt{A} \quad (29)$$

where T is the model parameter, and A is the area of the plate-soil contact patch.

For the same soil, the model parameter T remains the same and doesn't vary with the size of the plate. It was found that for contact areas ranging from 0.0005 to 0.25 m^2, the empirical model can be applied to dry sand and dry sandy loam with good agreement with experimental results. It is however not applicable to to wet loam and clay (M. Lyasko, 2010b).

Also, for the studies of settlement in classical soil mechanics, the soil can be treated as an elastoplastic material. When the pressure applied to the soil is small such that the stress in the soil below the load point (the location where the pressure is applied) doesn't pass the elastic limit of the stress-strain curve, the soil deformation can be regarded as elastic behavior. Assuming the soil to be semi-infinite, homogeneous, isotropic and elastic, Eq. (30), based on works of Boussinesq can be used to relate the sinkage to the pressure (Boussinesq, 1885):

$$p = \frac{2}{C_f}\frac{E}{1-\nu^2}\frac{z}{B} \tag{30}$$

where E is the Young's modulus, ν is the Poisson's ratio, B is a geometry parameter that characterizes the plate dimension, and C_f is the shape coefficient for the plate.

In cases of large pressure, where the stress in the soil exceeds a certain limit on the stress-strain curve, soil failure happens and the soil begins to collapse. The pressure which, if exceeded, results in soil failure is referred to as the bearing capacity. The bearing capacity can be characterized theoretically by (Terzaghi, 1944):

$$p = cN_c\lambda_c + \frac{B}{2}\gamma N_\gamma \lambda_\gamma + \gamma N_q \lambda_q z \tag{31}$$

where z is the vertical distance between the soil top surface and the place where the plate rests (depth of foundation), c is the cohesion of the soil, γ is the unit weight of the soil, λ_γ, λ_c, and λ_q are the shape coefficients of the plate, and N_c, N_γ, and N_q are the bearing capacity factors that are functions of soil friction angle ϕ and the shape coefficients λ_γ, λ_c, λ_q.

Kogure et al. proposed a theoretical pressure-sinkage model for the soil under a circular plate. The assumptions behind the model was that the normal pressure at a soil depth z, uniformly distributed at the same soil depth, was given by the ordinates of a paraboloid, and the ratio of normal pressure and vertical strain linearly decreases with the increase of the pressure. The model is given by (Kogure et al., 1983):

$$z = 2r\sqrt{\frac{p}{8CM_0}}\log\left(\frac{\sqrt{M_0}+\sqrt{2Cp}}{\sqrt{M_0}-\sqrt{2Cp}}\right) \tag{32}$$

where C and M_0 are the model parameters of linear function about the normal pressure and the vertical strain.

According to the works of Upadhyaya et al., Lyasko, and Ding et al. (Upadhyaya et al., 1993), (M. Lyasko, 2010b), (Ding et al., 2017), the model parameters of the classical empirical pressure-sinkage models are dependent on the running gear or plate dimensions, normal load levels and some other factors. They are thus non-invariant parameters. Also, all the aforementioned pressure-sinkage models describe the behavior of soil without hardpan. To characterize the

pressure-sinkage of soil using a few basic invariant soil parameters and taking into account the hardpan effect, Ageikin developed an analytical model that takes account soil hardpan effect (Ageikin, 1987a), (Ageikin, 1987b):

$$p = \frac{2EB_H z}{2Ez + \pi B_H A_o BJQ_1} \tag{33}$$

where E is the Young's modulus, B is the geometric parameter of the plate in contact with the soil, that is, the width (or smaller dimension) of a rectangular plate, or the radius of a circular plate, and model parameters B_H, Q, J and A_o are computed by:

$$B_H = \frac{B_i}{\arctan\left(\frac{\pi(H-z)}{2B}\right)} \tag{34}$$

$$B_i = \frac{L}{L+0.4B} \cdot \frac{\gamma g}{1000} \cdot \frac{1-S^4}{2S^5} \cdot B + \frac{L+B}{L+0.5B} 2C_o \frac{1+S^2}{S^3} + \frac{\gamma g}{1000S^2} z \tag{35}$$

$$S = \tan\left(\frac{\pi}{4} - \frac{\phi_o}{2}\right) \tag{36}$$

$$Q_1 = \frac{2}{\pi} \arctan\left(\frac{H-z}{A_o B}\right) \tag{37}$$

$$J = \frac{0.03 + L/B}{0.6 + 0.43L/B} \tag{38}$$

$$A_o = 0.64\left(1 + \frac{B}{H}\right) \tag{39}$$

where C_o is the soil cohesion, ϕ_o is the angle of soil internal shearing resistance, γ is the soil bulk density, B_i is the bearing capacities of soil with infinite hardpan H, B_H is the bearing capacities of soil with finite hardpan H, H is the hardpan depth, i.e., the thickness of upper soil layer that is relatively soft and can be deformed under a normal load, and L is the plate length.

Lyasko pointed out some limitations of the Ageikin model (M. Lyasko, 2010b). For example, the equation to compute the bearing capacities of soil with infinite hardpan in the Ageikin model cannot work for certain types of soil. The analytical model of stress distribution for the soil under a plate which provides the basis for the derivation of the Ageikin model falsely depends on average ground pressure. Resolving the limitations of the Ageikin model, Lyasko derived an analytical model given by (M. Lyasko, 2010b):

$$p = \frac{1}{\frac{D_1}{B_i} + \frac{D_2}{Ez}\omega B\xi} \tag{40}$$

where the model parameters D_1, D_2, ω, ξ, and B_i are computed by:

$$D_1 = \frac{2}{\pi}\arctan\left(\frac{\pi(H-z)}{2B}\right) \tag{41}$$

$$D_2 = \arctan\left(\frac{H-z}{A_o B}\right) \tag{42}$$

$$\omega = A_o J \quad (1.14 \le \omega \le 2.15) \tag{43}$$

$$\xi = 1 + 1.86\left(\frac{x}{2} + \frac{x^2}{3} - \frac{x^3}{5}\right) \tag{44}$$

$$x = 2.5\left(1 - \exp\left(-3.74B\right)\right) \tag{45}$$

$$B_i = \left[\exp\left(6.65\tan\phi_o - 1.75\right)\cdot\left(1 + 0.25\frac{B}{L}\right)B + \exp\left(4.76\tan\phi_o + 0.15\right)\cdot\left(1 + 1.5\frac{B}{L}\right)z\right]\frac{\gamma g}{1000}... \\ + \exp\left(3.32\tan\phi_o + 1.5\right)\left(1 + 0.3\frac{B}{L}\right)C_o \tag{46}$$

where ξ is the dimensionless contact pressure concentration coefficient, ω is the dimensionless coefficient, and other parameters and variables have the same meaning as that of the Ageikin model.

4.1.2 Pressure-sinkage models for non-zero slip

When slip occurs in the running gear-terrain or plate-terrain interface, tangential forces are generated perpendicular to the direction of normal pressure. This tangential force causes tangential deformation and the layer of soil in contact with the driven wheel or tire is "peeled" off and removed, causing slip sinkage. This phenomenon is more obvious in frictional soil than in completely cohesive soil (Reece, 1965). Reece found that when the running gear is operated on soil at non-zero slip, the sinkage is the sum of static sinkage and slip sinkage (Reece, 1965):

$$z = z_o + z_j \tag{47}$$

where z_o is the static sinkage, and z_j is the slip sinkage.

For the grouser-soil interaction, Reece proposed the following model to predict the slip including slip sinkage (Reece, 1964):

$$z = z_o + \frac{h_{gr} i}{1-i} \tag{48}$$

where h_{gr} is the grouser height, and i is the slip ratio.

Vasil'ev et al. applied the Bekker model in their study of sinkage at non-zero slip of running gear and devised an analytical model to determine the sinkage (Vasil'ev et al., 1969):

$$z = z_o + iH_p \tag{49}$$

where H_p is the depth of propagation of soil deformation which can be only evaluated experimentally.

Lyasko observed that these two models behave poorly at slip ratios higher than 35% as the sinkage computed with these two models is not in good agreement with the test data. The model proposed by Ksenevich et al. can predict sinkage at slip ratio ranging from 0% to 65% in an acceptable error from the test data (M. Lyasko, 2010c). The Ksecenevich et al. model was based on an assumption that when the rigid wheel is running on the soil, the work done by the pushing force can be equal to the vertical work done in deforming the soil, and the model is given by (Ksenevich et al., 1985):

$$z = \left(\frac{1+i}{1-0.5i} \right) z_o \tag{50}$$

Although the Bekker model and Reece model don't account for the slip sinkage, based on these classical empirical models, several empirical models have been proposed to work effectively for non-zero slip situations.

Gee-Clough modified the Bekker model by multiplying it by a function of slip to address the overestimation of the Bekker model in the case of deep sinkage and far-from-zero negative slip ratio (positive skid) (Gee-Clough, 1976):

$$p = \left(\frac{k_c}{b} + k_\phi \right) z^n \left(1+i\right)^{-n/(2n+1)} \tag{51}$$

where i is the skid of the wheel that makes the magnitude of the multiplier to the Bekker model smaller than 1.

Also by modifying the Bekker model, slip sinkage was taken into account in the Ding et al. model (Ding et al., 2010), (Gao et al., 2013). The sinkage exponent of the Bekker model was no longer a model parameter, but a linear function of slip ratio for positive slip and a quadratic function of slip for skid (negative slip) as given by:

$$p = \left(\frac{k_c}{b} + k_\phi \right) z^n \tag{52}$$

$$n = n_0 + n_1 s \qquad \text{if } s > 0 \tag{53}$$

$$n = n_0 + n_1 s + n_2 s^2 \qquad \text{if } s < 0 \tag{54}$$

where s is the slip ratio of the wheel, and n_0 , n_1 , and n_2 are model parameters in addition to the model parameters of the Bekker model.

The Ding et al. 2014 model, as described in Section 4.1.1., will be capable of predicting pressure and explicitly including slip ratio as a variable, if the dimensionless function is properly formulated. For cases of the positive slip, and the positive slip and negative slip with wheel lug effect considered, the dimensionless functions are given respectively by (Ding et al., 2014):

$$\lambda_N = \left(\frac{z}{z_0} \right)^{n_0 - 1 + n_1 s} \tag{55}$$

$$\lambda_N = \left(\frac{z}{z_0} \right)^{n_0 - 1 + n_1 s + n_2 s^2} \tag{56}$$

$$\lambda_N = \left(\frac{z}{z_0} \right)^{n_0 - 1 + n_1 s + n_2 s^2 + n_3 s^3} \tag{57}$$

where $z_0 = 1\text{m}$, s is the slip ratio of the wheel, and n_0 , n_1 , n_2 and n_3 are the function parameters.

It can be seen from the above dimensionless functions as functions of slip that only the influence of slip in the pressure-sinkage relationship (slip effect) is explicitly accounted for while other effects such as lug effects, running gear dimension effects, etc., are implicitly accounted. Parameterization of the dimensionless function for cases of positive slip (based on test results) showed the variation of n_0 and n_1 is not big among wheels of different dimensions (Ding et al., 2014).

To compute the radial stress along the wheel-soil interface in cases of non-zero slip, the pressure-sinkage model not only needs to account for the effect of slip, but also the maximum radial stress point. The position of the maximum radial stress point changes with the change in slip ratio, and the maximum radial stress angle can be a linear function of slip as shown below (Wong and Reece, 1967a):

$$\theta_M = (c_1 + c_2 i)\theta_1 \tag{58}$$

where θ_1 is the entry angle, i is the slip of the wheel, and c_1 and c_2 are model parameters.

4.1.3 Summary and model parameterization

The pressure-sinkage models introduced up to this point are summarized in Table 2, It should be noted that all the models listed in the table are static models and not dynamic models. Taking a fully parameterized Bekker model for example, when the pressure is given, the sinkage will be obtained by using the Bekker model as a constant value, not as a function of time. This means that the model cannot characterize how sinkage evolves with time under a given pressure. Unless the sinkage exponent is equal to one for certain types of soil, all the pressure-sinkage models represent pressure as a nonlinear function of sinkage for a steady-state penetration.

Most of the model parameters of the empirical and semi empirical pressure-sinkage models introduced above are non-invariant parameters (M. Lyasko, 2010b) except for the soil mechanics parameters and the soil physical property parameters. For a given soil condition, the non-invariant model parameters are dependent on plate dimensions, plate shapes, as well as penetration speed of the plate (Wong et al., 1982), (Upadhyaya et al., 1993), (Apfelbeck et al., 2011), (Ding et al., 2014). This partly explains the poor extrapolation of some empirical pressure-sinkage models, such as the Bekker model (Wong, 2008), because the plate-soil contact condition for parameterization of the model is different from that of application, and the use of the non-invariant model parameters with constant values can cause modelling errors.

The model parameters of the theoretical pressure-sinkage models introduced above are classical soil mechanics parameters and invariant parameters, i.e. the parameter value only depends on soil condition and not on plate-soil contact condition. Some of the theoretical pressure-sinkage models (e.g., the Lyasko model and the Ageikin model), though claimed to accurately represent the pressure-sinkage relationship with easier model parameterization than classical empirical and semi empirical models have not been applied to derive off-road tire/wheel dynamics model, possibly because of their complex form. The relatively simpler forms of the empirical and semi empirical pressure models makes it easy for them to be analytically integrated to calculate the vertical or horizontal wheel/tire force (Wong and Reece, 1967a), (Wong, 2008). This is not the case for the theoretical pressure-sinkage models with complex forms.

The parameterization methodologies for pressures-sinkage models are summarized in Table 3. For empirical and semi empirical models, the main test conducted in most of the parameterization methodologies is the sinkage test in which a plate or a cone penetrometer penetrates the soil, and the pressure and penetration depth are simultaneously recorded. Since the empirical and semi empirical models characterize steady state penetration, the penetration of the plate or cone in a sinkage test is preferably controlled to be a quasi-static penetration, i.e., with a constant penetration rate. In a sinkage test, the stress condition of soil is supposed to resemble the stress condition of the soil interacting with the running gear, which may explain why the cone penetrometer is not favored in most of the sinkage tests in this paper, as the cone-soil interaction doesn't resemble the running gear-soil interaction. Therefore, the selection of the plate size and plate shape tends to mimic the size and shape of the running gear-soil contact patch. Once the data about the pressure and the sinkage is obtained, depending on the form of the empirical and semi empirical model, in some cases, the model parameters can be calculated by using a few sets of data, e.g., the model parameters of the Eq. (14) (Kacigin and Guskovt, 1968); in most other cases, the model parameter can be determined by performing regression analysis, examples can be found in (Wong, 1980) and (Apfelbeck et al., 2011).

Occasionally when it comes to parameterizing the Bekker model or the Reece model incorporated into a semi empirical wheel dynamics model, e.g., in (Gao et al., 2013), the dynamic wheel-soil test is performed. In the test, the vertical wheel force and longitudinal wheel force are measured and recorded as part of the experimental data, and the experimental data is used in an optimization process where the model parameters of the Bekker model or Reece model are tuned such that the difference between the simulation result and the experimental data reaches a desirable range. The idea of this parameterization process is similar to the idea of the "Wheel Bevameter" (Plackett, 1985). Parameterization of empirical pressure-sinkage models that account for slip sinkage or steering effects requires dynamic wheel-soil testing at non-zero slip ratios or steering angle.

As for the parameterization of the theoretical pressure-sinkage model, the soil mechanics parameters need to be evaluated, and this can be done by routine classical soil mechanics experimental methodologies. Since the soil mechanics parameters are invariant parameters, parameterization is needed only once for one type of soil, unlike the fact that parameterization needs to be completed multiple times for one soil and plates of various shapes and sizes. However, among the model parameters of the theoretical pressure-sinkage models, there are soil cohesion and soil friction angle, the two model parameters of the Mohr-Coulomb failure model. It should be noted that even for the same soil, different shear tests can produce different evaluation results of the soil cohesion and soil friction angle (Okello, 1991). This can

cause difficulties in the parameterization of some theoretical pressure-sinkage models or may result in modelling errors when using them.

Table 2 Summary of pressure-sinkage models available in literature.

Model Parameters	**Model Nature**	**Slip Sinkage Effect**	**Steering Effect**	**Running Gear/Plate Size Effect**	**Hardpan Effect**	**Lug Effect**	**Unloading-reloading Effect**	**Equation No.**	**Reference**
k, n	Empirical	No	No	No	No	No	No	(1)	(Bernstein, 1913)
k, n	Empirical	No	No	Yes	No	No	No	(2)	(Saakyan, 1959)
k_c , k_ϕ , n	Empirical	No	No	Yes	No	No	No	(3)	(Bekker, 1969)
k_1 , k_2 , n	Empirical	No	No	Yes	No	No	No	(4)	(Onafeko and Reece, 1967)
k_c , k_ϕ , n , c , γ	Semi empirical	No	No	Yes	No	No	No	(5)	(Reece, 1965)
K_1 , K_2 , α , β , n	Semi empirical	No	No	Yes	No	No	No	(6)	(Youssef and Ali, 1982)
k_1 , k_2 , n , c_1 , c_2	Semi empirical	No	No	Yes	No	No	No	(7)	(Wong and Reece, 1967a)
$\hat{k}$, $\hat{m}$, $\hat{n}$	Empirical	No	No	Yes	No	No	No	(8)	(Meirion-Griffith and Spenko, 2011)
$\hat{k}$, $\hat{m}$, $\hat{n}$	Empirical	No	No	Yes	No	No	No	(9)(10)	(Meirion-Griffith and Spenko, 2013)
k_0, A_0, B_0	Semi empirical	No	No	Yes	No	No	No	(11)(12)	(Korchunov, 1948)
c, K	Semi empirical	No	No	Yes	No	No	No	(13)	(Evans, 1953)
k, p_0	Semi empirical	No	No	Yes	No	No	No	(14)	(Kacigin and Guskovt, 1968)

Model Parameters	Model Nature	Slip Sinkage Effect	Steering Effect	Running Gear/Plate Size Effect	Hardpan Effect	Lug Effect	Unloading-reloading Effect	Equation No.	Reference
C_m , s_0 , s_m , m	Empirical	No	No	Yes	No	No	No	(15)	(Gotteland and Benoit, 2006)
K_s, n_0, n_1	Empirical	No	No	No	No	No	No	(16)(17)	(Ding et al., 2014)
K_s, n_0, n_1, n_2	Empirical	No	No	No	No	No	No	(16) (18)	(Ding et al., 2014)
K_s, n_0, n_1	Empirical	No	No	Yes	No	No	No	(16) (19)	(Ding et al., 2014)
K_s, n_0, n_1, n_2	Empirical	No	No	No	No	No	No	(16) (20)	(Ding et al., 2014)
k_c , k_ϕ , n_0 , n_1 , α_1 , β_1	Empirical	No	Yes	Yes	No	No	No	(23)(24)	(Ding et al., 2017)
k_p , m_m	Semi empirical	No	No	Yes	No	No	No	(25)(26)	(Wong et al., 1982)
k_0 , A_u	Empirical	No	No	No	No	No	Yes	(27)(28)	(Wong et al., 1984)
T	Empirical	No	No	No	No	No	No	(29)	(Tsytovich, 1963)
E, v	Theoretical	No	No	Yes	No	No	No	(30)	(Boussinesq, 1885)
c, ϕ, γ	Theoretical	No	No	Yes	No	No	No	(31)	(Terzaghi, 1944)
C, M_0	Theoretical	No	No	Yes	No	No	No	(32)	(Kogure et al., 1983)
C_o , ϕ_o, γ, E	Theoretical	No	No	Yes	Yes	No	No	(33) - (39)	(Ageikin, 1987a), (Ageikin, 1987b)
C_o , ϕ_o, γ, E	Theoretical	No	No	Yes	Yes	No	No	(40) - (46)	(M. Lyasko, 2010b)

Model Parameters	Model Nature	Slip Sinkage Effect	Steering Effect	Running Gear/Plate Size Effect	Hardpan Effect	Lug Effect	Unloading-reloading Effect	Equation No.	Reference
N/A	Empirical	Yes	No	No	No	Yes	No	(48)	(Reece, 1964)
H_p	Empirical	Yes	No	No	No	No	No	(49)	(Vasil'ev et al., 1969)
N/A	Theoretical	Yes	No	No	No	No	No	(50)	(Ksenevich et al., 1985)
k_c, k_ϕ, n	Semi-empirical	Yes	No	Yes	No	No	No	(51)	(Gee-Clough, 1976)
k_c, k_ϕ, n_0, n_1	Empirical	Yes	No	Yes	No	No	No	(52)(53)	(Ding et al., 2010)
k_c, k_ϕ, n_0, n_1, n_2	Empirical	Yes	No	Yes	No	No	No	(52)(54)	(Gao et al., 2013)
K_s, n_0, n_1	Empirical	Yes	No	No	No	No	No	(16)(55)	(Ding et al., 2014)
K_s, n_0, n_1, n_2	Empirical	Yes	No	No	No	Yes	No	(16)(56)	(Ding et al., 2014)
K_s, n_0, n_1, n_2, n_3	Empirical	Yes	No	No	No	Yes	No	(16)(57)	(Ding et al., 2014)

Table 3 Summary of parameterization methodologies for the pressure-sinkage models.

Experimental Methodology	Employed Instruments	Parameter Determined	Soil Type	Equation No.	Reference
Sinkage test	Bevameter with circular plate and Rammsonde cone	n, k_ϕ, k_c / k, n	Snow	(3) (1)	(Wong and Irwin, 1992)
Sinkage test	Test rig driven by a dc motor that is equipped with a force transducer, rotary potentiometer, etc., and circular plates	n, k_ϕ, k_c	Sand	(3)	(McKyes and Fan, 1985)
Sinkage test	Bevameter with automatic data processing unit and circulate plates	n, k_ϕ, k_c / k_c, k_ϕ, n, c, γ	Snow, sand	(3) (5)	(Wong, 1980)

Experimental Methodology	Employed Instruments	Parameter Determined	Soil Type	Equation No.	Reference
Sinkage test	Penetration-shear device, combined, sinkage plates	k, n n, $ck_c + \gamma k_\phi b$	Loam	(1) (5)	(Upadhyaya et al., 1993)
Sinkage test	Grenoble sinkage equipment with circular plate powered by hydraulic ram	m, C_m, s_m s_0 n, k_ϕ, k_c	Silty sand, sand, silt	(15)	(Gotteland and Benoit, 2006)
Sinkage test	Vehicle-mounted bevameter with circular and rectangular plates, portable automatic data-processing system	k_p, m_m, k_o, A_u	Muskeg	(25)(26)	(Wong et al., 1982)
Sinkage test	Bevameter with circular and rectangular plates	n, k_ϕ, k_c	Sand, clay	(3)	(Apfelbeck et al., 2011)
Sinkage test	Tractor-mounted bevameter with circular, oval, and rectangular plates	n, k_ϕ, k_c	Loam	(3)	(Massah and Noorolahi, 2010)
Sinkage test	Hydraulic Bevameter with rectangular plate	k, n c, ϕ, γ	Sand	(1) (31)	(Onafeko and Reece, 1967)
Sinkage test	Circular and rectangular plates	K_1, K_2, α, β, n	Sand, clayey sand	(6)	(Youssef and Ali, 1982)
Dynamic wheel-soil test	Wheel test rig, load cells	c_1, c_2	Sand	(58)	(Wong and Reece, 1967a),
Sinkage test	Pressure-sinkage testbed that includes a wheel section, force sensor, and linear actuator and potentiometer	$\hat{k}$, $\hat{m}$, $\hat{n}$	Sand, calcium silicate, earth	(8)	(Meirion-Griffith and Spenko, 2011)
Sinkage test	Pressure-sinkage testbed that includes a wheel section, force sensor, and linear actuator and potentiometer	$\hat{k}$, $\hat{m}$, $\hat{n}$	Kaolin clay/silt mix	(9)(10)	(Meirion-Griffith and Spenko, 2013)
Sinkage test	N/A	p_0, k	Sandy loam, loam, clay	(14)	(Kacigin and Guskovt, 1968)

Experimental Methodology	**Employed Instruments**	**Parameter Determined**	**Soil Type**	**Equation No.**	**Reference**
Dynamic wheel-soil test	Wheel–soil interaction testbed that is equipped with a displacement sensor, a six-axis F/T sensor, a torque sensor, etc.	K_s, n_0, n_1	Sand	(16)(55)	(Ding et al., 2014)
		K_s, n_0, n_1, n_2		(16)(56)	
		K_s, n_0, n_1, n_2, n_3		(16)(57)	
Sinkage test	Wheel–soil interaction testbed equipped with a circular plate, displacement sensor, F/T sensor, etc.	K_s, n_0, n_1	Sand	(16) (19)	(Ding et al., 2014)
		n , k_ϕ , k_c		(3)	
Sinkage test	Circular plates	K_s, n_0, n_1, n_2	Sand	(16) (20)	(Ding et al., 2014), (Reece, 1964)
		n , k_ϕ , k_c		(3)	
Dynamic wheel-soil steering test	Wheel–soil interaction testbed that is equipped with a displacement sensor, a six-axis F/T sensor, a torque sensor, etc.	k_c , k_ϕ , n_0 , n_1 , α_1 , β_1	Sand	(23)(24)	(Ding et al., 2017)
Sinkage test	Circular and rectangular plates	T	Sandy loam, sand, clay, loam, clayey sand	(29)	(M. Lyasko, 2010b), (Bekker, 1969), (Wills, 1966), (Hvorslev, 1970), (Sela and Ehrlich, 1972), (Rusanov, 1998), (Youssef and Ali, 1982), (Reece, 1964)
		n , k_ϕ , k_c		(3)	
Sinkage test	Rectangular plates	k, p_0	Sand, loam, clay	(14)	(M. Lyasko, 2010b), (Wills, 1966),
Sinkage test	Rectangular and circular plates	m , C_m , s_m s_0	Sand	(15)	(M. Lyasko, 2010b), (Sela and Ehrlich, 1972)
Sinkage test	Rectangular and circular plates	C_o , ϕ_o, γ, E	Sand, sandy loam, clay, loam	(40) - (46)	(M. Lyasko, 2010b), (Bekker, 1969), (Wills, 1966), (Rusanov, 1998), (Reece, 1964)
Dynamic wheel-soil test, sinkage test	Wheel–soil interaction testbed that is equipped with a circular plate, a displacement sensor, a six-axis F/T sensor, a torque sensor, etc.	k_c , k_ϕ , n_0 , n_1 , n_2	Sand	(52)(54)	(Gao et al., 2013)

4.2 Shear stress-displacement models

Beside the pressure-sinkage model, another fundamental model in the study of running gear-soil interaction is the shear stress-displacement model. With the geometry of the running gear-soil interface known and these two models fully parameterized, the thrust due to the shear stress, the motion resistance due to the pressure, and the drawbar pull that is the difference between the thrust and the motion resistance can be computed.

Shear stress-displacement models are used to determine the tangential interactive stress in the running gear-soil or plate-soil interface. The tangential interactive stress causes the soil flow under the interface. For the running gear, the integral of tangential interactive stress provides thrust, and part of the vertical reaction force to balance the normal load. Regardless of the magnitude of the shear displacement, a maximum shear stress (the shear strength) exists and is governed by the Mohr-Coulomb failure criterion, as shown below:

$$\tau_{\max} = c + \sigma \tan\phi \tag{59}$$

where τ_{max} is the maximum shear strength that leads to soil failure, c is the soil cohesion, and ϕ is the angle of soil internal shearing resistance (soil friction angle).

Eq. (59) (The Mohr-Coulomb equation) is not the only equation used to determine the maximum shear stress when soil failure happens. Several modified versions of the equation above were proposed in the past to accurately model the shear strength for clay (Sun et al., 2006), for unsaturated soil (Hilf, 1956), and for partially saturated soil (Bishop et al., 1960). However, because of its adequate characterization of the shear strength and the simplicity of its form, the Mohr-Coulomb equation is widely (perhaps the most widely) used in the terramechanics community. It is incorporated into many semi empirical shear stress-displacement models, and it provides the basis for derivation of some semi empirical shear stress-displacement models, which is introduced in the rest of this section.

The three earliest pioneers were M. G. Bekker, G. I. Pokrovski, and Z. Janosi who laid the foundation for the development of the shear stress-displacement model. For the soil with a shear stress-displacement profile that displays a maximum shear stress (a hump), Bekker developed the following model (Bekker, 1956), (Bekker, 1969):

$$\tau = \tau_{\max} \times \frac{\left\{\exp\left[\left(-K_2 + \sqrt{K_2^2 - 1}\right) K_1 j\right] - \exp\left[\left(-K_2 - \sqrt{K_2^2 - 1}\right) K_1 j\right]\right\}}{\left\{\exp\left[\left(-K_2 + \sqrt{K_2^2 - 1}\right) K_1 j_0\right] - \exp\left[\left(-K_2 - \sqrt{K_2^2 - 1}\right) K_1 j_0\right]\right\}} \tag{60}$$

where τ is the shear stress, j is the shear displacement, τ_{max} is the shear strength that can be characterized by the Mohr-Coulomb equation, j_0 is the shear displacement at the maximum shear stress τ_{max}, and K_1 and K_2 are empirical model parameters. Wong pointed out that determining the values of K_1 and K_2 for the Bekker shear stress-displacement model is involved (Wong and Preston-Thomas, 1983).

For most types of soil, at a very high level of shear displacement, the shear stress remains almost at a constant value even though the shear displacement increases. Prokovski proposed a model to represent this feature of the shear-stress displacement profile (Pokrovski, 1937):

$$\tau = \left[C_1 \exp\left(-C_2 j\right) + C_3\right] \times \left[1 - \exp\left(-C_4 j\right)\right] \tag{61}$$

where C_1, C_2, C_3, and C_4 are the empirical model parameters.

Some shear stress-displacement profiles don't have a hump. The shear stress increases with the shear displacement and then approaches a constant value. This feature was observed for the internal shearing of dry sand, saturated clay, fresh snow and peat, and plate-soil shearing of sand, peat, snow and muskeg (Kacigin and Guskovt, 1968), (Wong and Preston-Thomas, 1983), (Okello, 1991). To describe these shear stress-displacement relationships, Janosi and Hanomoto modified the Bekker model, resulting in (Janosi, 1961):

$$\tau = \tau_{\max}\left[1 - \exp\left(-j/K\right)\right] \tag{62}$$

where K is the shear deformation modulus.

It is worth noting that when setting C_1 of the Pokrovksi model to zero and treating C_3 to be the maximum shear stress, the Pokrovski and the Janosi and Hnaomoto models are equivalent. The Pokrovski model actually works for both the shear stress-displacement profile with a hump and that without a hump. The premise is that both have a constant shear stress at a high level of shear displacement. Inspired by the Pokrovski model, Kacigin and Guskovt developed a shear stress-displacement as shown below (Kacigin and Guskovt, 1968):

$$\tau = \tau_{res}\left[1 + \frac{a}{\cosh\left(j/K_\omega\right)}\right]\tanh\left(j/K_\omega\right) \tag{63}$$

$$a = 2.55\left(\frac{\tau_{\max}}{\tau_{res}} - 1\right)^{0.825} \tag{64}$$

where τ_{res} is the residual stress and it has a constant value at which the shear stress remains regardless of the increase in the shear displacement, a is the model parameter, K_ω is the shear displacement where the shear stress reaches its maximum.

Later, Oida found that the Kacigin and Guskovt model only works for the case where the ratio of maximum shear stress to the residual stress is 2.7554. Oida proposed a corrected model based on the Pokrovski model (Oida, 1975):

$$\tau = \tau_{\max} K_r \times \left[1 - \frac{\sqrt{1-K_r}\exp\left(\frac{j}{K_\omega}\log\left(1+\frac{\sqrt{1-K_r}-1}{K_r}\right)\right)}{\sqrt{1-K_r}\left(1-2/K_r\right)+2/K_r-2} \right] \times \left[1-\exp\left(\frac{j}{K_\omega}\log\left(1+\frac{\sqrt{1-K_r}-1}{K_r}\right)\right)\right] \quad (65)$$

where K_ω is the shear displacement where the shear stress reach its maximum, and K_r is the ratio of the residual shear stress τ_{res} to the maximum shear stress τ_{max}.

The Oida model applies only to the shear stress-displacement profile with a hump and residual stress. This kind of profile was observed for certain types of loam and snow covers (Wong, 2009). Because of the complex form of the Oida model, its parameterization using the experimental shear stress-displacement data was found to be an involved process, especially to identify the proper value of K_r (Wong and Preston-Thomas, 1983). To overcome this obstacle, inspired by the Pokrovski model, the following model was proposed by Wong (Wong and Preston-Thomas, 1983):

$$\tau = \tau_{\max} K_r \left\{ 1+\left[\frac{1}{K_r\left(1-1/e\right)}-1 \right] e^{(1-j/K_\omega)} \right\} \cdot \left[1-e^{(-j/K_\omega)} \right] \quad (66)$$

For a shear stress-displacement profile with a hump and a residual stress, Sela hypothesized that the shear stress-displacement model consists of two functions, one due to soil cohesion and the other due to soil friction angle (Sela, 1964). Two functions may be respectively from experimental shear stress-displacement curve for two types of soil. One is completely cohesive and the other is completely frictional. Although without experimental data for validation, Sela hypothesizes that those two functions are given by Eqs. (67) and (68):

$$\tau_c = c\frac{j}{d_c}\exp\left(1-\frac{j}{d_c}\right) \quad (67)$$

$$\tau_\phi = p\tan\phi\left[1-\exp\left(\frac{j}{d_\phi}\right)\right] \quad (68)$$

$$\tau = \tau_c + \tau_\phi \tag{69}$$

where p is the normal pressure on the shear plane, d_c is the shear displacement at the maximum cohesive shear stress, and d_ϕ is the frictional displacement constant.

Influenced by Sela's hypothesis (Sela, 1964) and noticing different shear behaviors of Mojave mars soil simulant at the same normal stress yet different soil density, Senatore and Iagnemma proposed the following shear stress-displacement model that accounts for the influence of the soil density on the shear stress-displacement curve (Senatore and Iagnemma, 2011):

$$\tau = \tau_{res}\left[\frac{k_\gamma j}{k}\exp(1-j/k) + \left(1-\exp(-j/k)\right)\right] \tag{70}$$

where k_γ is the model parameter related to the influence of soil density on the shear stress, and k is a model parameter.

For some organic type of soil (e.g., muskeg mat) the shear stress-displacement profile has a hump without a residual stress. In other words, after reaching the maximum shear stress, the shear stress will continually decrease with an increase of shear displacement. Wong et al. suggested the following model for this type of shear stress behavior (Wong et al., 1979):

$$\tau = \tau_{\max}\left(\frac{j}{K_\omega}\right)\exp\left(1-\frac{j}{K}\right) \tag{71}$$

where K_ω is the shear displacement where the shear stress reaches its maximum.

Later, Lyasko found that by proper selection of values of model parameters, the Pokrovski model can also be used to portray the shear stress-displacement profile for those aforementioned organic types of soil (M. I. Lyasko, 2010).

Ageikin thought model parameters such as K_r, K_ω, and τ_{max} are non-invariant plate-soil paramters, and their values can vary with the shear plate size for a given soil condition. With an attempt to use invariant soil parameters as model parameters, Ageikin proposed the shear stress-displacement model below. The model parameters of the Mohr-Coulomb equation and two soil shear parameters are the invariant model parameters for the Ageikin model, and their values remain the same at a given soil condition regardless of the shear plate size and geometry (Ageikin, 1987a), (Ageikin, 1987b), (Ageikin, 1992).

$$\tau = \frac{1}{\frac{1}{\varsigma c + \mathrm{p}\cdot\tan(\phi)} + \frac{t_{gr}}{E'\cdot|j|}}$$

$$\varsigma = \begin{cases} 0 & \text{if} \quad \dfrac{j}{t_{gr}} < K' \\ 1 - \dfrac{m'\cdot j}{t_{gr}} & \text{if} \quad \dfrac{j}{t_{gr}} > K' \end{cases} \tag{72}$$

where t_{gr} is the grouser pitch, c is the soil cohesion, p is the applied average ground pressure, φ is the soil friction angle, and m' and E' are soil shear parameters.

The shear stress-displacement models are summarized in Table 4. It can be seen from Table 4 that the maximum shear stress needs to be determined to parameterize the shear stress-displacement model. As previously mentioned, the Mohr-Coulomb equation is widely used to represent the maximum shear stress for the shear stress-displacement model. Many traditional soil mechanics experimental methodologies can be applied for the parameterization of the Mohr-Coulomb equation. Therefore, together with these soil mechanics methodologies, the parameterization methodologies for the shear stress-displacement models are listed in Table 5.

Table 4 Summary of shear stress-displacement available in literature.

Model Parameters	**Model Nature**	**Applicable Shear Stress-Displacement Curve Feature**	**Equation No.**	**Reference**
τ_{maxs}, K	Semi empirical	A	(62)	(Janosi, 1961)
$\tau_{\max}$, K_ω	Semi empirical	B	(71)	(Wong et al., 1979)
C_1 , C_2 , C_3 , C_4	Empirical	A, B, C	(61)	(Pokrovski, 1937)
$\tau_{\max}$, j_0 , K_1 , K_2	Semi empirical	B, C	(60)	(Bekker, 1969)
d_c, d_ϕ, c, ϕ	Semi empirical	C	(67)(68)(69)	(Sela, 1964)
$\tau_{\max}$, τ_{res} , K_ω ,	Semi empirical	A, C	(63)(64)	(Kacigin and Guskovt, 1968)
$\tau_{\max}$, K_ω , K_r	Semi empirical	C	(65)	(Oida, 1975)
$\tau_{\max}$, K_ω , K_r	Semi empirical	C	(66)	(Wong and Preston-Thomas, 1983)
τ_{res}, k_γ, k	Semi empirical	C	(70)	(Senatore and Iagnemma, 2011)

c, ϕ, m', E'	Semi empirical	A, C	(72)	(Ageikin, 1987a), (Ageikin, 1987b), (Ageikin, 1992)

Shear Stress-Displacement Curve Feature No.	**Description**
A	No hump, shear stress increases with the shear displacement until reaches an asymptote at large shear displacement.
B	A hump of maximum shear stress, to the right of the hump, shear stress continually decreases with the increase of shear displacement.
C	A hump of maximum shear stress, to the right of the hump, shear stress decreases with the increase of shear displacement until reaches a residual stress.

Table 5 Summary of parameterization methodologies for the shear stress-displacement model and the Mohr-Coulomb equation available in literature.

Experimental Methodology	**Employed Instruments**	**Parameter Determined**	**Soil Type**	**Equation No.**	**Reference**
Direct shear test	Modified direct shear box	ϕ	Sand	(59)	(Cerato and Lutenegger, 2006), (Guo, 2008)
Direct shear test	Modified direct shear apparatus	c, ϕ	Clay loam	(59)	(Gan et al., 1988)
Direct shear test	Direct shear testing machine	c, ϕ, K	Loam	(59) (62)	(Godbole et al., 1993)
Direct shear test	Direct shear box	c, ϕ, K	Mojave Martian Simulant	(59) (62)	(Smith, 2014)
Direct shear test	Direct shear box	ϕ	Sand	(59)	(Matsuoka et al., 2001)
Triaxial test	Triaxial test apparatus.	ϕ	Sand	(59)	(Baker, 2004),
Triaxial test	Triaxial test apparatus.	c, ϕ	Clay	(59)	(Baker, 2004), (Peterson, 1988)

Triaxial test	Triaxial test apparatus.	c, ϕ	Sandy clay	(59)	(Rahardjo et al., 2004),
Unconfined compression test	Unconfined compression test apparatus.	c	Clay	(59)	(Kamei and Iwasaki, 1995); (Matsuoka et al., 2001); (Campbell and Hudson, 1969)
Vane shear test	Miniature vane shear	c	Clay	(59)	(Bolton et al., 1993)
Vane shear test	Shear vane	c	Sandy clay, loam, clay, sandy loam	(59)	(Okello, 1991)
Vane shear test	Shear vane	c	Clay loam, clay, silt clay loam	(59)	(Sridharan and Prakash, 1999)
Shear test	Bevameter	c, ϕ, K	Loam	(59) (62)	(Park et al., 2008)
Torsional shear test	Bevameter, circular grouser	c, ϕ	Sand, silt	(59)	(Apfelbeck et al., 2011)
Torsional shear test	Bevameter with automatic data processing unit, annular shear plates with grouser	c, ϕ, K, K_ω, K_r	Sand, snow, muskeg, sandy loam, clayey loam, loam,	(59) (65) (66) (71)	(Wong, 1980), (Wong et al., 1984), (Wong, 2009)
Torsional shear test	Wheel–soil interaction testbed, shearing plate with grouser	c, ϕ, K	Sand	(59) (62)	(Gao et al., 2013)
Translational shear test	Penetration-shear device, combined, grouser plates	c, ϕ, K	Loam	(59) (62)	(Upadhyaya et al., 1993)

Among the traditional soil mechanics methodologies for shear strength of soil, the vane shear test cannot be used to evaluate the soil friction angle because when shearing of the soil happens as the vane is in a rotation, the normal stress to the soil in the shearing movement is zero; only the direct shear test can be used to parameterize the shear stress-displacement model, because only the direct shear test can record the shear displacement. However, the direct shear tests listed in Table 5 are only applicable to the internal shearing of soil and not to the plate-shearing of soil. In terramechanics, the plate-shearing of soil is important for the study of traction performance of wheel-soil and tire-soil interaction. By contrast, the bevameter can be used to investigate both the internal shearing of soil and plate-shearing of soil depending on the profile of the chosen shearing plate mounted to the bevameter. When conducting the shear test for

the parameterization of the shear stress-displacement model, the size, shape and profile of the shearing plate or the size of the direct shear box, and the shearing rate need to be properly selected in order to accurately capture the feature of the running gear-soil interaction to be modelled. It is suggested that the rule of thumb is to make sure the shear behavior in the shear test needs to closely resemble the shear behavior of the running gear-soil interface to be modelled in terms of type of shearing (i.e., internal shearing of soil or the plate-shearing of soil) and of shear rate (i.e., the shear rate may need to be equal to the slip velocity of the running gear to be modelled) (Wong et al., 1984). The type of shearing and the shear rate clearly influence the model parameterization results according to the data collected by Wong (Wong, 2009). Table 5 also indicates that to determine the same set of parameters for the same type of soil, more than one methodology can be applied. For example, both the torsional shear test using a Bevameter and the direct shear test using the direct shear box can be performed to the loam such that the cohesion, the soil friction angle, and the shear deformation modulus are evaluated. However, this fact doesn't mean the evaluation result will be the same for these two experimental methodologies. For example, to determine the value of the soil cohesion which Lyasko call the invariant soil parameter (M. Lyasko, 2010b), different traditional soil mechanics experimental methodologies applied to the same soil led to different values of the soil cohesion (Okello, 1991). The diversity of the shear test methodologies causes difficulties not only in the correct selection of parameterization methodologies for the shear stress-displacement model or for the shear strength model, but also in comparing the terramechanics research results.

4.3 Running gear-terrain or plate-terrain vibration models

Running gear-terrain or plate-terrain vibration models are used to model the interaction between running gears and terrain or plates and terrain due to vibration induced by the motion of the running gear or the plate. As introduced next, these models can either predict the soil compaction, the displacement of the wheel axle, or the interactive force, or account for phenomenon caused by vibration that occur in the running gear-terrain interface. This approach to modelling is relatively recent and testing procedures and equipment are yet to be standardized.

Hildebrand et al. proposed two models based on both a linear method and a rheologically-based non-linear method to study the vehicle vibrations, soil vibrations and soil compaction as the vehicle traverses the soft terrain (Hildebrand et al., 2008). Surface profile variation, tire and suspension features, and soil parameters were taken as the model input. In the linear model, the tire-soil contact force, the soil response, vehicle response and the soil sinkage can be captured respectively by:

$$F(\omega) = K_{sys}(\omega)Y(\omega) \tag{73}$$

$$S_{FF}(\omega) = \left|K_{sys}(\omega)\right|^2 S_{YY}(\omega) \tag{74}$$

$$Y_{soil}(\omega) = \frac{F(\omega)}{K_{soil}(\omega)} \tag{75}$$

$$S_{Y_{soil}Y_{soil}}(\omega) = \frac{S_{FF}(\omega)}{\left|K_{soil}(\omega)\right|^2} \tag{76}$$

$$Y_{veh}(\omega) = \frac{F(\omega)}{K_{veh}(\omega)} \tag{77}$$

$$S_{Y_{veh}Y_{veh}}(\omega) = \frac{S_{FF}(\omega)}{\left|K_{veh}(\omega)\right|^2} \tag{78}$$

$$Y_c(\omega) = \frac{\varepsilon_{c,proc}}{\varepsilon_{e,proc}} Y_{soil}(\omega) \tag{79}$$

$$S_{Y_cY_c}(\omega) = \left|\frac{\varepsilon_{c,proc}}{\varepsilon_{e,proc}}\right|^2 S_{Y_{soil}Y_{soil}}(\omega) \tag{80}$$

where F is the tire-soil contact force, S_{FF} is the spectral density of tire-soil contact force, Y_{soil} is the soil displacement response, $S_{Y_{soil}Y_{soil}}$ is the spectral density of soil displacement, Y_{veh} is the vehicle displacment response, $S_{Y_{veh}Y_{veh}}$ is the spectral density of vehicle displacement, Y_c is the soil compaction displacement, and $S_{Y_cY_c}$ is the spectral density of soil compaction displacement.

The model parameters of the equations above are the dynamic stiffness of the soil and vehicle in series K_{sys}, the soil dynamic stiffness K_{soil}, the vehicle dynamic stiffness K_{veh}, the non-recoverable strain per cycle of the Proctor test $\varepsilon_{c,proc}$, and the elastic strain per cycle of the Proctor test $\varepsilon_{e,proc}$. The equation to calculate the vehicle dynamic stiffness depends on how the vehicle is modelled analytically. Such equations for a rigid wheel and half-axle are given in Eqs. (81) and (82), yet the equation to calculate the vehicle dynamic stiffness for a unsuspended vehicle with compliant and damped tires is more complex, and readers interested can refer to (Hildebrand et al., 2008).

$$K_{veh} = -M_u\omega^2 \tag{81}$$

$$K_{veh} = \frac{k_{tire}\left(1+i\eta_{tire}\right)\omega^2}{\omega^2 - \omega_{veh}^2} \tag{82}$$

where M_u is the unsprung mass (the mass of tire and axle), ω is the circular frequency of the wheel, k_{tire} is the static tire stiffness, ω_{veh} is the natural frequency of vehicle mass on tire compliance, and η_{tire} is the tire loss factor.

To calculate the dynamic stiffness of soil, the soil is treated as a bed of springs that are not independent but a part of a continuous medium, and the solution of the point receptance (the inverse of the soil dynamic stiffness that excludes the loss factor) of an elastic half-space is given by the integral as shown in Eqs. (83) - (85). The assumption behind this approach is that the wavelength is larger than the size of the tire-soil contact patch at the frequency range of interest (Hildebrand et al., 2008).

$$\alpha = -\frac{2c_P^2}{\rho c_S^4}\left\{\int_0^{\zeta_0-\delta}\frac{\sqrt{\zeta^2-1}}{\Gamma(\zeta)}\frac{\left[\mathrm{J}_1\left(\zeta k_P r\right)^2\right]}{\zeta k_P r}d\zeta - \int_{\zeta_0+\delta}^{\infty}\frac{\sqrt{\zeta^2-1}}{\Gamma(\zeta)}\frac{\left[\mathrm{J}_1\left(\zeta k_P r\right)^2\right]}{\zeta k_P r}d\zeta + \mathrm{Res}\right\} \tag{83}$$

$$\mathrm{Res} = -\frac{\pi i\sqrt{\zeta_0^2-1}}{\Gamma'(\zeta_0)}\frac{\mathrm{J}_1\left(\zeta_0 k_P r\right)^2}{\zeta_0 k_P r} \tag{84}$$

$$\Gamma(\zeta) \equiv \left(2\zeta^2 - \left(\frac{c_P}{c_S}\right)^2\right)^2 - 4\zeta^2\left(\zeta^2-1\right)^{\frac{1}{2}}\left(\zeta^2 - \left(\frac{c_P}{c_S}\right)^2\right)^{\frac{1}{2}} \tag{85}$$

Where α is the point receptance of soil for excitation under tire by a force distributed uniformly over conctact zone, ζ_0 is the root of $\Gamma(\zeta)$, δ is the vanishing parameter, k_P is the P-wave number, r is the radius of tire-soil contact patch, and J_1 is the Bessel function of the first-order.

Besides the approach above to treat soil as a bed of springs, the equation to calculate the soil dynamic stiffness incorporates a high-strain loss factor η that is calculated by assuming a linear stress-strain cycle per blow of the Proctor test (hence, the model is named the "linear model"), as shown in Eqs. (86) - (91). The loss factor is the imaginary component of the soil dynamic stiffness K_{soil}, and represents damping. The loss factor is correlated with some soil parameters that can be evaluated by the modified proctor test and seismic test.

$$K_{soil} = \frac{1+i\eta}{\alpha} \tag{86}$$

$$\eta \equiv \frac{E_{c,proc}}{2\pi E_{e,proc}} = \frac{D}{\pi}\frac{\varepsilon_{c,proc}^2}{E_{c,proc}} \tag{87}$$

$$\varepsilon_{c,proc} = \frac{1}{\sqrt{125}}\left(1 - \frac{\gamma_d}{\gamma_{d,\max}}\right) \tag{88}$$

$$D = \frac{2G(1-\nu)}{(1-2\nu)} \tag{89}$$

$$G = \rho c_S^2 \tag{90}$$

$$\nu = \frac{c_P^2 - 2c_S^2}{2\left(c_P^2 - c_S^2\right)} \tag{91}$$

Where

- $E_{c,proc}$ is the specific energy per blow of the Proctor test,
- D is the soil bulk modulus of elasticity,
- G is the shear modulus of the soil,
- ν is the Poisson's ratio of soil,
- c_S is the S-wave speed of soil,
- c_P is the P-wave speed of soil,
- ρ is the density of soil,
- γ_d is the dry specific weight of soil, and
- $\gamma_{d,max}$ is the dry specific weight of soil attainable in a modified Proctor compaction test.

Once the soil dynamic stiffness and the vehicle dynamic stiffness are known, the soil-vehicle system dynamic stiffness can be obtained by

$$K_{sys}(\omega) = \frac{K_{soil}K_{veh}}{K_{soil} + K_{veh}} \tag{92}$$

The linear model described above loses validity for very soft soil whose damping level is correspondingly very high. To cope with the very high damping level, a non-linear model based on the Rheological model was developed. This non-linear model treats the soil as a non-linear viscous-thixotropic dashpot connected in series with a linear dynamic stiffness element, as shown below by (Hildebrand et al., 2008)

$$K_{soil} = \left[\alpha_{hs}(\omega) + \frac{1}{i\omega C_{eq}(F,\omega)} \right]^{-1} \tag{93}$$

where $\alpha_{hs}(\omega)$ is the point receptance of a half-space to a force distributed uniformly over circular area, and C_{eq} is the equivalent linear damping coefficient.

The set of equations Eq. (83) – (85) that give solution to the inverse of the soil dynamic stiffness (the point receptance) that excludes the loss factor also works for the linear dynamic stiffness element of the non-linear model, which means $\alpha_{hs}(\omega)$ can be computed the same way as using Eq. (83) – (85) to compute α. The equivalent linear damping coefficient is related to the time-average power dissipation by the viscous-thixotropic damping $\bar{W}$, as indicated by the Eq. (94):

$$C_{eq} = \frac{1}{2} \frac{|F|^2}{\bar{W}} \tag{94}$$

$$\bar{W} = \bar{W}_{R>r} + \bar{W}_{R\le r} \tag{95}$$

$$\bar{W}_{R\le r} = \frac{1}{2} aB\omega^m \cos\frac{m\pi}{2} p^{2+m} \left(\frac{2}{3}\pi r^3 \right) \tag{96}$$

$$\bar{W}_{R>r} = \frac{1}{2} aB\omega^m \cos\frac{m\pi}{2} \frac{(3F)^{2+m}}{(2\pi)^{1+m}} \left(\frac{r^{-1-2m}}{1+2m} \right) \left(\frac{1}{3} - \frac{m}{12} \right) \tag{97}$$

where *a*, *B*, *m* are the soil rheological parameter, and *p* is the average pressure over the tire-soil contact zone.

Cuong et al. modelled the tire-soil interaction as a single degree of freedom (DOF) mass-spring-damper system and studied the influence of tire inflation pressure, soil moisture content, depth of test soil, and tire normal load on the damping ratio (Cuong et al., 2014). The equation of motion for the tire-soil interaction system is:

$$\ddot{z} + 2\xi\omega_n \dot{z} + \omega_n^2 z = 0 \tag{98}$$

$$\omega_n = \sqrt{\frac{k_{eq}}{m_{eq}}} \tag{99}$$

$$\xi = \frac{c_{eq}}{2\sqrt{m_{eq} k_{eq}}} \tag{100}$$

Where z is the displacement of wheel axle, ω_n is the undamped natural angular frequency, ξ is the damping ratio, m_{eq} is tire load, equivalently the static and dynamic wheel normal load, k_{eq} is the equivalent stiffness constant of tire-soil system, and c_{eq} is the equivalent damping coefficient of tire-soil system.

In on-road tire dynamics, a single DOF mass-spring-damper system has been widely used to study the vertical vibration of the tire on a rigid road (Wong, 2008). The spring constant/characteristic (if nonlinear) and the damping coefficient are regarded as the function of tire properties. By contrast, the single DOF mass-spring-damper system applied by Cuong et al. assumes that the spring constant and damping coefficient are influenced not only by tire properties but also by soil properties (Cuong et al., 2014). Hence, the spring constant is called the equivalent stiffness constant, unlike the spring constant for on-road tire dynamics named called the stiffness of the tire.

Irani et al. conducted a dynamic wheel-soil test in which a rigid smooth wheel moved in a straight line at a constant wheel normal load (applied by the dead weight) and at a preset wheel slip ratio that was controlled around a given value. As for the test result, it was found that the measured drawbar pull fluctuated around a mean value with time, and the rut profile after the traffic had cyclic peaks and troughs. Irani et al. claimed that the models based on traditional terramechanics approach cannot explain the drawbar pull fluctuations. To account for these fluctuations, a dynamic pressure-sinkage model with an empirical vibration term for the smooth wheel-soil interface was developed as shown below (Irani et al., 2010):

$$p(z) = \left(\frac{k_c}{b} + k_\phi \right) z^n + A \sin\left(\omega t + \Phi \right) \tag{101}$$

where k_c, k_ϕ and n are the model parameters of the Bekker model, A is the amplitude of the pressure oscillations, ω is the frequency of the oscillations, and Φ is the phase shift.

The frequency of the oscillations is empirically modeled as a linear function of the wheel slip ratio:

$$\omega(i) = k_i i + C \tag{102}$$

where i is the wheel slip ratio, and k_c and C are empirical model parameters.

Eqs. (101) - (102) were incorporated into a semi empirical wheel dynamic model, and the model parameterization was completed to the empirical vibration term of Eq. (101) by using the test data from the dynamic wheel-soil test. The drawbar pull computed by the semi empirical wheel dynamic model matched the measured drawbar pull within an acceptable errors (Irani et al., 2010). The authors of this paper think Eqs. (101) - (102) don't explain physically why the

pressure under the wheel in motion fluctuates with time. Although Irani et al. claimed the fluctuation in the drawbar pull cannot be accounted for by traditional terramechanics approach, proof about this claim was not given in (Irani et al., 2010). Hence the possibility that traditional terramechanics approach could account for the fluctuation in the drawbar pull measured in the dynamic wheel-soil test is not ruled out. Since the test soil could be inhomogeneous, the authors of this paper think the values of the k_c and k_φ in the Bekker model might not have constant values everywhere in the test soil. Therefore, even the wheel normal load has a constant value prescribed by the dead weight, the geometry of the wheel-soil interface, i.e., the maximum soil sinkage right beneath the wheel center, the entry angle, etc., might vary as the wheel moves longitudinally. The variation in the geometry of the wheel-soil interface could lead to the variation or fluctuation in the drawbar pull.

For the wheel with grousers, Irani et al. modified the model as shown by Eqs. (101) - (102) to account for the fluctuation in drawbar pull, vertical soil reaction force, and wheel sinkage observed in the dynamic wheel-soil test (Irani et al., 2011). The modified model is:

$$p(z) = \left(ck_c' + \gamma b k_\phi'\right)\left(\frac{z}{b}\right)^n + A\sin\left(\omega t + \Phi\right) \quad (103)$$

where c, k_c', γ, b, and k_φ' are the model parameters of the Reece pressure-sinkage model.

Compared with Eq. (102), the frequency of the oscillations is not dependent on the slip ratio but on the the number of wheel grousers n_g and the angular velocity of the wheel ω_w, and is given by:

$$\omega = \frac{\omega_w}{n_g} \quad (104)$$

Besides, unlike the model for smooth wheel, the amplitude factor A doesn't have a constant value at given slip ratio and normal load, but consists of two terms respectively due to passive compression and active expansion of the soil interacting with the grouser, and to the change in soil density during the grouser-soil interaction, as shown by:

$$A = A_\sigma + A_\gamma \quad (105)$$

$$A_\sigma = k_g' \bar{\sigma}_p \quad (106)$$

$$A_\gamma = k_a' l_c d\gamma \quad (10

7)

where A_σ is the factor related to the active and passive stresses due to the grouser-terrain interaction, A_γ is the factor related to the change in local soil density around the wheel and grouser because of the soil deformation, $k_g^{'}$ is an empirical model parameter, $\bar{\sigma}_p$ is the mean of the passive stresses from the grousers in contact with the terrain, $k_a^{'}$ is an empirical model parameter, l_c is the contact length, and $d\gamma$ is the change in weight density of the soil.

A semi empirical wheel model that incorporated Eqs. (103) - (107) was found to capture the experimental data about drawbar pull, vertical soil reaction force, and wheel sinkage within acceptable errors at 66 N wheel normal load. However, this semi empirical model couldn't produce results that matched the experimental data at 15 N wheel normal load. Irani et al. explained that the model parameters of Eqs. (106) - (107) were tuned at 66 N wheel normal load, hence these values of model parameters were not supposed to produce good simulation results at 15 N wheel normal load that was hugely different from 66 N wheel normal load (Irani et al., 2011).

Table 6 summarizes the aforementioned vibration models in terms of model parameters, analysis domain and output parameters. These vibration models, unlike the pressure-sinkage empirical model and the shear displacement-shear stress model, are a collection of theoretical model that can be analyzed either from the time domain or the frequency domain. These vibration models only characterize the vibration in the vertical direction, and hence they have the potential to be extended for the study of vehicle ride comfort over the soft soil. The experimental methodologies to parameterize the vibration models are briefed in

Table 7. Test ideas for the parameterization come from vibration theory, wave propagation and traditional soil property tests.

Table 6 Vibration models for soil compaction available in literature.

Model Name	**Analysis Domain**	**Model Parameters**	**Model Outputs**	**Equation No.**	**Reference**
Single DOF mass-spring-damper model for tire-soil system	Time domain	ω_n , ξ	z	(98) –(100)	(Cuong et al., 2014)
Non-linear tire-soil interaction model	Time domain	a , B , m , ρ , c_S , c_P	Y_{soil} , Y_{veh} , Y_c , F	(73) - (92)	(Hildebrand et al., 2008)

Linear tire-soil interaction model	Frequency domain	γ_d , $\gamma_{d,\max}$, ρ , $E_{c,proc}$, c_S , c_P	Y_{soil} , Y_{veh} , Y_c , F	(73) - (85), (92) - (97)	(Hildebrand et al., 2008)
Dynamic pressure-sinkage model for a smooth wheel	Time domain	k_c, k_φ, n, C, A, Φ, k_i,	p	(101) - (102)	(Irani et al., 2010)
Dynamic pressure-sinkage model for a wheel with grousers	Time domain	c, k'_c, γ, k'_φ, k'_g, k'_a, Φ,	p	(103) - (107)	(Irani et al., 2011)

Table 7 Parameterization of vibration models for soil compaction.

Experimental Methodology	**Employed Instruments**	**Parameter Determined**	**Soil Type**	**Equation No.**	**Reference**
Free vibration logarithm decay method	Vibration Test Rig, a single-direction accelerometer	ξ	Sandy loam	(98) –(100)	(Cuong et al., 2014)
Modified proctor test, seismic test, measurement of soil density	hammer, sample cylinder, SASW and/or refraction seismics, scale	a , B , m , c_S , c_P	clay	(73) - (92)	(Hildebrand et al., 2008)
Measurement of dry bulk density, modified Proctor test, seismic test	Oven, scale, hammer, sample cylinder, SASW and/or refraction seismics	γ_d , $\gamma_{d,\max}$, ρ , $E_{c,proc}$, c_S , c_P	Clay, loam	(73) - (85), (92) - (97)	(Hildebrand et al., 2008)
Dynamic wheel-soil test	Single wheel testbed with a JR3 6 d. o. f. transducer, a FUTEK torque sensor, and a linear potentiometer	C, A, k_i,	Sand	(101) - (102)	(Irani et al., 2010)
Dynamic wheel-soil test	Single wheel testbed with a JR3 6 d. o. f. transducer, a FUTEK torque sensor, and a linear potentiometer	k'_g, k'_a	Sand	(103) - (107)	(Irani et al., 2011)

Parameterization of either the linear or the non-linear version of the tire-soil interaction vibration model, requires the seismic test to determine the S-wave speed and P-wave speed of the soil to be modelled. Performing the modified

Proctor test is also needed, yet its procedures slightly differ between parameterization of linear model and that of non-linear model. In the modified Proctor test, for the linear model, the maximum dry bulk density is measured, while for the non-linear model, the final compaction strain is measured and recorded as a reference value. Using the non-linear model, simulation of the modified Proctor test is run for several times during which the soil rheological model parameters a, B, and m are varied such that the final compaction strain obtained from the simulation result will reach the reference value (Hildebrand et al., 2008).

Free decaying vibration tests are performed to parameterize the model applied by Cuong et al. The test tire drops from a height of 200mm to the test soil surface. After impacting the test soil and under the constraint of the vertical slide guide bar, the test tire starts free-decay vibration. The vertical acceleration and vertical displacement of the test tire are recorded, and the Free-vibration logarithm decay method is applied to the recorded data for the evaluation of the damping ratio.

Measurements of drawbar pull and rut profile from dynamic wheel-soil tests are needed to parameterize the dynamic pressure-sinkage model proposed by Irani et al. for a smooth wheel. From the multiple plots of drawbar pull vs time obtained from the test at various levels of slip ratio, the values of frequency of the oscillations ω are identified for each of the test slip ratios, and the model parameters of Eq. (102) are determined by using linear regression analysis. The values of the amplitude factor A are manually tuned such that the drawbar pull computed by the semi empirical wheel dynamics model that incorporates Eqs. (101) - (102) fits the drawbar pull measured in the test (Irani et al., 2010). Similar parameterization method can be applied to the dynamic pressure-sinkage model for the wheel with grousers proposed by by Irani et al. The model parameters of Eqs. (106) - (107) $k_g^{'}$ and $k_a^{'}$ are tuned to make the simulation results match the experimental results (Irani et al., 2011). However, for both dynamic pressure-sinkage models, how the value of the phase shift Φ is determined was not described in (Irani et al., 2010), (Irani et al., 2011).

5. Emerging techniques applicable to a real-time terramechanics environment

As mentioned in the Introduction, real-time applications may assist in estimating states, parameters, and properties used to model the terrain-vehicle interaction. This section highlights several parameters needed to model: 1) sinkage and slip of some running gear or of some implement; and 2) forces or pressures acting on the running gear or implement

5.1 Sinkage and slip measurement

Measurement of the sinkage while operating an off-road vehicle or using earthmoving machinery comprises of two parts, an elastic sinkage (or deformation) and a plastic sinkage (or deformation). This is very difficult to measure separately and the elastic region of the sinkage has to be inferred in post processing from measured forces. The forces applied during these tests are usually quasi-static of nature. Botha, Els, Shoop, Becker, and Sopher (Botha et al., 2016) developed a three-dimensional spatial measurement technique that can be used to measure the rut profile behind a rolling wheel. The measurement technique utilizes several inexpensive webcams to capture images of the soil in front of and behind a moving wheel. The cameras placed in front of the wheel measure the undisturbed terrain and the cameras behind the wheel measure the ensuing rut after the wheel has passed. This measurement technique is capable of measuring the three-dimensional rut profile with an accuracy of approximately 1mm. At this stage, the measurement technique is not capable of processing the image data in real-time, but it is expected that sufficient advances in both the algorithm and processing power may soon result in this technique being suitable for real-time application. This rut profile measurement technique enables one to measure the plastic deformation of the soil with relative ease. Figure 1 shows a typical result of measuring the rut depth in sand.

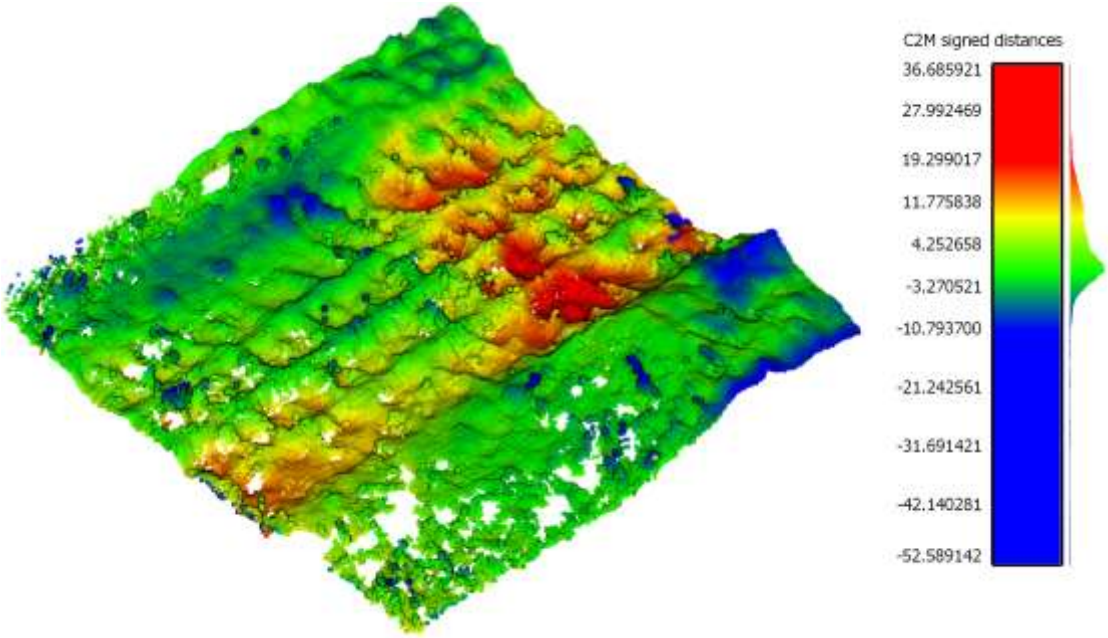

Figure 1. The deformed point cloud with a colour map applied to represent the relative distance to the undeformed profile

Measurement of the elastic deformation is considerably more complex, as it has to be measured in situ with the wheel obstructing the view. Guthrie, Botha, Jimenez, Els & Sandu (Guthrie et al., 2017) investigated a novel approach to measuring the elastic deformation by inserting two webcams into the wheel. The webcams are between the rim and the tyre and are oriented so that the contact patch area is in view constantly. The experimental setup is called the Tyre-Terrain Camera System (T2CAM) and is shown in Figure 2. A mechanical mechanism stabilizes the cameras to ensure that the contact patch is permanently in view.

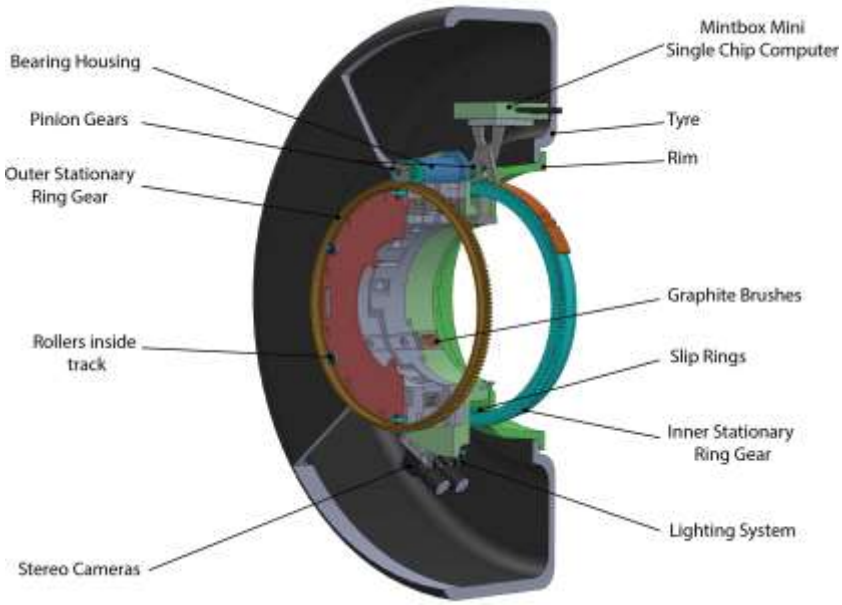

Figure 2. T2CAM imaging system used to measure tire contact patch deformation

By measuring the contact patch deformation and assuming that the tire rubber compound is much stiffer than the soil, one can get a good estimate of the sinkage while the wheel is moving over the soil. Assuming that the total sinkage is a combination of the elastic and plastic deformation, the elastic sinkage can be separated from the plastic sinkage. Using the T2CAM to measure the elastic sinkage of soft terrain is still work in progress, but is already delivering promising results. Several updates to the T2CAM are planned, including the addition of more sensors to allow for some validation of the experimental results.

When slip (longitudinal and lateral) is present in the tire-terrain interface, accurate slip measurement is also of utmost importance. Using digital image correlation techniques, Botha and Els (Botha and Els, 2015a), Botha and Els (Botha and Els, 2015b), developed a measurement capability that can directly measure the longitudinal and lateral slip conditions in the tire-terrain interface. Johnson, Botha and Els (Johnson et al., 2017) extended this approach to measure

the side-slip angle of a vehicle in real-time and hence these approaches may be used to measure the tire-terrain slip directly, in real-time.

5.2 Force measurement

The measurement of forces and moments has been well established in the literature. There are numerous examples of wheel force transducers available on the commercial market, although these wheel force transducers are typically very expensive and designed for relatively low loads. The loads are typically associated with that experienced by a passenger vehicle. The Vehicle Dynamics Group at the University of Pretoria designed and tested a wheel force transducer that makes use of six individual single component load cells to measure the forces and moments acting on a tire (Becker and Els, 2012). The original design was for 16 inch rims, but the design has recently been scaled to account for very large off-road tyres. The updated wheel force transducers have a static load rating of 150 kN and a dynamic load rating of 300 kN.

The wheel force transducer design is intended to be integrated with the T2CAM, thus providing all six forces and moments acting on the wheel along with the full field deformation of the undisturbed terrain, the contact patch deformation and the subsequent rut form by the wheel. The wheel force transducer is designed to fit 29 inch rims and is shown in Figure 3.

Figure 3. The 29 inch wheel force transducers with static load rating of 150 kN

6. Conclusion and future work

Although terramechanics has incorporated theoretical concepts and experimental methodologies from traditional soil mechanics and vehicle engineering, each of which has its own standards, the ISTVS mainly considers the terrain-

vehicle interaction research that has specific needs. These specific needs require a well-defined, cohesive, and consistent set of standards. Thus, the objective of this study is to support an update and enhancement of the ISTVS standards. The first step was to conduct a literature survey on the soil parameters and parameterization methodologies for fundamental terramechanics models. This phase also produced a large collection and classification of published studies related to soil parameters measurement and soil modeling techniques. The use of terramechanics modelling in the emerging field of real-time measurement was also discussed.

A few conclusions can be drawn from the work conducted for this study so far. There is no reference method for the parameterization of most terramechanics fundamental models. Furthermore, multiple experimental methods could be used to parameterize the same terramechanics model; however, the results of one method may differ from those obtained with another method, and it is hard to know which one is more accurate. Thus, the difficulty of establishing standards for terramechanics tests is increased due to such challenges. Also, it can be seen that the experimental methodologies for the parameterization of the pressure-sinkage empirical models, and the shear displacement-shear stress models rely mostly on the plate-sinkage tests and soil shear tests. These two types of tests may need to be standardized in ISTVS standard. Also, attention needs to be paid to which types of soil need to be tested in order to validate a newly proposed model, this aspect might also be specified in a future ISTVS standard. For the vibration models, their parameterization methodologies have included ideas from other disciplines and are still evolving. In this case, the conventional experimental methodologies are insufficient, and more research is needed to produce standards useful for terramechanics studies.

Recent emerging technologies, such as digital image correlation techniques and the development of wheel force transducers capable of withstanding very high loads, may bring a new dawn in the world of terramechanics. The imaging techniques have the ability to provide full field deformation in front of, inside and behind a rolling tire, while the large wheel force transducers are capable of measuring forces up to 300 kN.

Future work will be focused on clearly stating the proposed related updates for the ISTVS standards for soil properties and mobility of vehicles on soil, as well as creating the repositories for all the soil parameters, testing facilities, and other information collected during the project. On top of that, an open database of soil properties and testing facilities will be built for the ISTVS community.

Acknowledgements

This study has been partially supported by the ISTVS Research Award, the U.S. Army Engineer Research and Development Center (ERDC), the European Union Horizon 2020 Framework Program, Marie Skłodowska Curie actions, Project EVE, "Innovative Engineering of Ground Vehicles with integrated Active Chassis Systems", the Vehicle Dynamics Group at University of Pretoria, the Terramechanics, Multibody, and Vehicle Systems (TMVS) Laboratory at Virginia Tech, and the NSF I/UCRC Center for Tire Research (CenTiRe).

References

Ageikin, J.S., 1992. Physical and mathematical soil parameters for evaluation of wheeled vehicle–terrain interaction, in: Proceedings of the International Symposium "Optimal Interaction." Russian Terramechanics Committee, Syzdal, Russia, pp. 3–9.

Ageikin, J.S., 1987a. Off-the-road wheeled and combined traction devices: theory and calculation. New Delhi: Amerind Pub. Co., New Delhi.

Ageikin, J.S., 1987b. Off-the-road mobility of automobiles. New Delhi: Amerind Pub. Co., New Delhi.

Apfelbeck, M., Kuß, S., Rebele, B., Schäfer, B., 2011. A systematic approach to reliably characterize soils based on Bevameter testing. J. Terramechanics 48, 360–371. https://doi.org/10.1016/j.jterra.2011.04.001

ASAE, 1999. Procedures for Using and Reporting Data Obtained with the Soil Cone Penetrometer, ASAE EP542 FEB1999 (R2013). American Society of Agricultural and Biological Engineers, St. Joseph, Michigan.

Ayers, P., Perumpral, J., 1982. Moisture and density effect on cone index. Trans. ASAE 25, 1169–1172. https://doi.org/10.13031/2013.33691

Baker, R., 2004. Nonlinear Mohr Envelopes Based on Triaxial Data. J. Geotech. Geoenvironmental Eng. 130, 498–506. https://doi.org/10.1061/(ASCE)1090-0241(2006)132:1(130)

Becker, C.M., Els, P.S., 2012. Wheel force transducer measurements on a vehicle in transit, in: Proceedings of the 12th European Regional Conference of the ISTVS. Pretoria, South Africa.

Bekker, M.G., 1969. Introduction to Terrain-Vehicle Systems. Part I: The Terrain. Part II: The Vehicle. University of Michigan, Ann Arbor, Michigan.

Bekker, M.G., 1956. Theory of land locomotion: the mechanics of vehicle mobility. The University of Michigan Press, Ann Arbor, Michigan.

Bernstein, R., 1913. Probleme zur experimentellen Motorpflugmechanik. Der Mot. 16, 199–206.

Bishop, A.W., Alpan, I., Blight, G.E., Donald, I.B., 1960. Factors controlling the strength of partly saturated cohesive soils, in: Research Conference on Shear Strength of Cohesive Soils. Boulder, CO, pp. 503–532.

Bolton, M.D., Gui, M.W., Phillips, R., 1993. Review of Miniature Soil Probes For Model Tests, in: Eleventh Southeast Asian Geotechnical Conference. pp. 85–90.

Boon, N.E., Yahya, A., Kheiralla, A.F., Wee, B.S., Gew, S.K., 2005. A tractor-mounted, automated soil penetrometer-shearometer unit for mapping soil mechanical properties. Biosyst. Eng. 90, 381–396. https://doi.org/10.1016/j.biosystemseng.2004.12.004

Botha, T.R., Els, P.S., 2015a. Digital image correlation techniques for measuring tyre-road interface parameters: Part 1 - Side-slip angle measurement on rough terrain. J. Terramechanics 61, 87–100. https://doi.org/10.1016/j.jterra.2015.04.004

Botha, T.R., Els, P.S., 2015b. Digital image correlation techniques for measuring tyre-road interface parameters: Part 2 - Longitudinal tyre slip ratio measurement. J. Terramechanics 61, 101–112. https://doi.org/10.1016/j.jterra.2015.05.003

Botha, T.R., Els, P.S., Shoop, S.A., Becker, C.M., Sopher, A., 2016. Three-dimensional rut profile measurement in snow and mud, in: Proceedings of the 8th ISTVS Americas Regional Conference. Troy, MI.

Boussinesq, J., 1885. Application des potentiels à l'étude de l'équilibre et du mouvement des solides élastiques: principalement au calcul des déformations et des pressions que produisent, dans ces solides, des efforts quelconques exercés sur une petite partie de leur surface. Gauthier-Villars, Paris.

Campbell, D.B., Hudson, W.R., 1969. The Determination of Soil Properties in Situ. Austin, Texas.

Cerato, A.B., Lutenegger, A.J., 2006. Specimen size and scale effects of direct shear box tests of sands. Geotech. Test. J. 29, 507–516. https://doi.org/10.1520/GTJ100312

Cuong, D.M., Zhu, S., Ngoc, N.T., 2014. Study on the variation characteristics of vertical equivalent damping ratio of tire–soil system using semi-empirical model. J. Terramechanics 51, 67–80. https://doi.org/10.1016/j.jterra.2013.10.002

Ding, L., Gao, H., Deng, Z., Li, Y., Liu, G., 2014. New perspective on characterizing pressure-sinkage relationship of terrains for estimating interaction mechanics. J. Terramechanics 52, 57–76. https://doi.org/10.1016/j.jterra.2014.03.001

Ding, L., Gao, H., Deng, Z., Tao, J., 2010. Wheel slip-sinkage and its prediction model of lunar rover. J. Cent. South Univ. Technol. 17, 129–135. https://doi.org/10.1007/s11771−010−0021−7

Ding, L., Yang, H., Gao, H., Li, N., Deng, Z., Guo, J., Li, N., 2017. Terramechanics-based modeling of sinkage and moment for in-situ steering wheels of mobile robots on deformable terrain. Mech. Mach. Theory 116, 14–33. https://doi.org/10.1016/j.mechmachtheory.2017.05.011

Evans, I., 1953. The sinkage of tracked vehicles on soft ground. Br. J. Appl. Phys. 4, 330–334.

Freitag, D.R., 1966. A dimensional analysis of the performance of pneumatics tires on clay. J. Terramechanics 3, 51–68. https://doi.org/10.1016/0022-4898(66)90106-6

Gan, J.K.M., Fredlund, D.G., Rahardjo, H., 1988. Determination of the shear strength parameters of an unsaturated soil using the direct shear test. Can. Geotech. J. 25, 500–510. https://doi.org/10.1139/t88-055

Gao, H., Guo, J., Ding, L., Li, N., Liu, Z., Liu, G., Deng, Z., 2013. Longitudinal skid model for wheels of planetary exploration rovers based on terramechanics. J. Terramechanics 50, 327–343. https://doi.org/https://doi.org/10.1016/j.jterra.2013.10.001

Gee-Clough, D., 1976. The Bekker theory of rolling resistance amended to take account of skid and deep sinkage. J. Terramechanics 13, 87–105. https://doi.org/10.1016/0022-4898(76)90016-1

Gee-Clough, D., Sommer, M.S., 1981. Steering forces on undriven, angled wheels. J. Terramechanics 18, 25–49. https://doi.org/10.1016/0022-4898(81)90016-1

Godbole, R., Alcock, R., Hettiaratchi, D., 1993. The prediction of tractive performance on soil surfaces. J. Terramechanics 30, 443–459. https://doi.org/10.1016/0022-4898(93)90036-W

Gotteland, P., Benoit, O., 2006. Sinkage tests for mobility study, modelling and experimental validation. J. Terramechanics 43, 451–467. https://doi.org/10.1016/j.jterra.2005.05.003

Guo, P., 2008. Modified Direct Shear Test for Anisotropic Strength of Sand. J. Geotech. Geoenvironmental Eng. 134, 1311–1318. https://doi.org/10.1061/(ASCE)1090-0241(2008)134:9(1311)

Guthrie, A.G., Botha, T.R., Jimenez, E., Els, P.S., Sandu, C., 2017. Dynamic 3D measurement of tyre-terrain interaction, in: 19th International and 14th European-African Regional Conference of the ISTVS. Budapest.

Hildebrand, R., Keskinen, E., Navarrete, J.A.R., 2008. Vehicle vibrating on a soft compacting soil half-space: Ground vibrations, terrain damage, and vehicle vibrations. J. Terramechanics 45, 121–136. https://doi.org/10.1016/j.jterra.2008.09.003

Hilf, J.F., 1956. An investigation of pore water pressure in compacted cohesive soils. Denver, CO.

Hvorslev, M.J., 1970. The basic sinkage equations and bearing capacity theories.

Irani, R.A., Bauer, R.J., Warkentin, A., 2011. A dynamic terramechanic model for small lightweight vehicles with rigid wheels and grousers operating in sandy soil. J. Terramechanics 48, 307–318. https://doi.org/10.1016/j.jterra.2011.05.001

Irani, R.A., Bauer, R.J., Warkentin, A., 2010. Modelling a Single-Wheel Testbed for Planetary Rover Applications, in: ASME 2010 Dynamic Systems and Control Conference. Cambridge, Massachusetts, USA, pp. 181–188. https://doi.org/10.1115/DSCC2010-4079

Ishigami, G., 2008. Terramechanics-based analysis and control for lunar/ planetary exploration robots. TOHOKU UNIVERSITY.

Jain, A., Balaram, J., Cameron, J., Guineau, J., Lim, C., Pomerantz, M., Sohl, G., 2004. Recent developments in the ROAMS planetary rover simulation Environment. IEEE Aerosp. Conf. Proc. 2, 861–876. https://doi.org/10.1109/AERO.2004.1367686

Janosi, Z., 1961. The analytical determination of drawbar-pull as a function of slip for tracked vehicles in deformation soils, in: Proc. of the 1st Int. Conf. of Terrain-Vehicle Systems. Torino, Italy.

Johnson, D.K., Botha, T.R., Els, P.S., 2017. Real-time slip angle measurements using digital image correlation, in: 19th International and 14th European-African Regional Conference of the ISTVS. pp. 1–8.

Kacigin, V. V, Guskovt, V. V, 1968. The basis of tractor performance theory: Part 1—General laws of soil strength and deformation. J. Terramechanics 5, 43–66. https://doi.org/10.1016/0022-4898(68)90080-3

Kamei, T., Iwasaki, K., 1995. Evaluation of Undrained Shear Strenght of Cohesive Soils Using a Flat Dilatometer. Soils Found. 35, 111–116.

Kogure, K., Ohira, Y., Yamaguchi, H., 1983. Prediction of sinkage and motion resistance of a tracked vehicle using plate penetration test. J. Terramechanics 20, 121–128. https://doi.org/10.1016/0022-4898(83)90043-5

Korchunov, S.S., 1948. Nesushazia sposobnost i deformasia nizinnoi zaleji. Gosenergoizdat.

Ksenevich, I.P., Skotnikov, V.A., Lyasko, M.I., 1985. Undercarriage systems; soil; crop. Moscow: Agropromizdat, Moscow.

Linström, B.V., Els, P.S., Botha, T.R., 2018. A real-time non-linear vehicle preview model. Int. J. Heavy Veh. Syst. 25, 1–22. https://doi.org/10.1504/IJHVS.2018.089893

Lyasko, M., 2010a. Multi-pass effect on off-road vehicle tractive performance. J. Terramechanics 47, 275–294. https://doi.org/10.1016/j.jterra.2010.05.006

Lyasko, M., 2010b. LSA model for sinkage predictions. J. Terramechanics 47, 1–19. https://doi.org/10.1016/j.jterra.2009.06.004

Lyasko, M., 2010c. Slip sinkage effect in soil-vehicle mechanics. J. Terramechanics 47, 21–31. https://doi.org/10.1016/j.jterra.2009.08.005

Lyasko, M.I., 2010. How to calculate the effect of soil conditions on tractive performance. J. Terramechanics 47, 423–445. https://doi.org/10.1016/j.jterra.2010.04.003

Madsen, J., Negrut, D., Reid, A., Seidl, A., Ayers, P., Bozdech, G., Freeman, J., O'Kins, J., 2012. A Physics-Based Vehicle/Terrain Interaction Model for Soft Soil Off-Road Vehicle Simulations. SAE Int. J. Commer. Veh. 5, 280–290. https://doi.org/10.4271/2012-01-0767.

Massah, J., Noorolahi, S., 2010. Design, development and performance evaluation of a tractor-mounted bevameter. Soil Tillage Res. 110, 161–166. https://doi.org/10.1016/j.still.2010.07.002

Matsuoka, H., Liu, S., Sun, D., Nishikata, U., 2001. Development of a New In-Situ Direct Shear Test. Geotech. Test. J. 24, 92–102. https://doi.org/10.1520/GTJ11285J

McKyes, E., Fan, T., 1985. Multiplate penetration tests to determine soil stiffness moduli. J. Terramechanics 22, 157–162. https://doi.org/10.1016/0022-4898(85)90050-3

Meirion-Griffith, G., Spenko, M., 2013. A pressure-sinkage model for small-diameter wheels on compactive, deformable terrain. J. Terramechanics 50, 37–44. https://doi.org/10.1016/j.jterra.2012.05.003

Meirion-Griffith, G., Spenko, M., 2011. A modified pressure-sinkage model for small, rigid wheels on deformable terrains. J. Terramechanics 48, 149–155. https://doi.org/10.1016/j.jterra.2011.01.001

Meyerhof, G.G., 1951. The ultimate bearing capacity of foundations. Geotechnique 2, 301–332.

Oida, A., 1975. Study on equation of shear stress-displacement curves. J. JAPANESE Soc. Agric. Mach. 37, 20–25.

Okello, A., 1991. A review of soil strength measurement techniques for prediction of terrain vehicle performance. J. Agric. Eng. Res. 50, 129–155. https://doi.org/10.1016/S0021-8634(05)80010-1

Onafeko, O., Reece, A.R., 1967. Soil stresses and deformations beneath rigid wheels. J. Terramechanics 4, 59–80. https://doi.org/10.1016/0022-4898(68)90021-9

Osman, M.S., 1964. The mechanics of soil cutting blades. Trans. ASAE 9, 318–328.

Park, W.Y., Chang, Y.C., Lee, S.S., Hong, J.H., Park, J.G., Lee, K.S., 2008. Prediction of the tractive performance of a flexible tracked vehicle. J. Terramechanics 45, 13–23. https://doi.org/10.1016/j.jterra.2007.11.002

Peterson, R.W., 1988. Interpretation of triaxial compression test results on partially saturated soils. Adv. Triaxial Test. Soil Rock, ASTM STP 977 512–538. https://doi.org/10.1520/STP29096S

Plackett, C.W., 1985. A review of force prediction methods for off-road wheels. J. Agric. Eng. Res. 31, 1–29. https://doi.org/10.1016/0021-8634(85)90122-2

Pokrovski, G.I., 1937. Issledovanie no fizike gruntov.

Rahardjo, H., Heng, O.B., Choon, L.E., 2004. Shear strength of a compacted residual soil from consolidated drained and constant water content triaxial tests. Can. Geotech. J. 41, 421–436. https://doi.org/10.1139/t03-093

Reece, A.R., 1965. Principles of soil-vehicle mechanics. Proc. Inst. Mech. Eng. Automob. Div. 180, 45–46. https://doi.org/10.1243%2FPIME_AUTO_1965_180_009_02

Reece, A.R., 1964. Problems of soil vehicle mechanics. Warren, Michigan.

Rula, A.A., Nuttall, C.J., 1971. An analysis of ground mobility models (ANAMOB). Vicksburg, Mississippi.

Rusanov, V.A., 1998. A problem of soil compaction by vehicles and how to solve it. Moscow: VIM., Moscow.

Saakyan, S.S., 1959. Vzaimodeistrie vedomogo kolesa i pochvi.

Sandu, C., Kolansky, J., Botha, T.R., Els, P.S., 2015. Multibody Dynamics Techniques for Real-Time Parameter Estimation, in: NATO Science for Peace and Security Series D: Information and Communication Security. IOS Press, pp. 221–241. https://doi.org/10.3233/978-1-61499-576-0-221

Savitski, D., Schleinin, D., Ivanov, V., Augsburg, K., Jimenez, E., He, R., Sandu, C., Barber, P., 2017. Improvement of traction performance and off-road mobility for a vehicle with four individual electric motors: Driving over icy road. J. Terramechanics 69, 33–43. https://doi.org/10.1016/j.jterra.2016.10.005

Schreiber, M., Kutzbach, H.D., 2008. Influence of soil and tire parameters on traction. Res. Agric. Eng. 54, 43–49.

Sela, A.D., 1964. The shear stress-deformation relationship of soils. J. Terramechanics 1, 31–37. https://doi.org/10.1016/0022-4898(64)90122-3

Sela, A.D., Ehrlich, I.R., 1972. Load support capability of flat plates of various shapes in soils. J. Terramechanics 8, 39–69. https://doi.org/10.1016/0022-4898(72)90094-8

Senatore, C., Iagnemma, K., 2011. Direct shear behaviour of dry, granular soils for low normal stress with application to lightweight robotic vehicle modelling, in: Proceedings of the 17th ISTVS International Conference. Blacksburg, Virginia.

Sloss, D., 1977. International society for terrain-vehicle systems standards. J. Terramechanics 14, 153–182. https://doi.org/10.1016/0022-4898(77)90013-1

Smith, W., 2014. Modeling of Wheel-Soil Interaction for Small Ground Vehicles Operating on Granular Soil. University of Michigan.

Sridharan, a, Prakash, K., 1999. Mechanisms controlling the undrained shear strength behaviour of clays. Can. Geotech. J. 36, 1030–1038. https://doi.org/10.1139/cgj-36-6-1030

Sun, D., Yao, Y.P., Matsuoka, H., 2006. Modification of critical state models by Mohr-Coulomb criterion. Mech. Res. Commun. 33, 217–232. https://doi.org/10.1016/j.mechrescom.2005.05.006

Taheri, Sh., Sandu, C., Taheri, S., Pinto, E., Gorsich, D., 2015. A technical survey on Terramechanics models for tire-terrain interaction used in modeling and simulation of wheeled vehicles. J. Terramechanics 57, 1–22. https://doi.org/10.1016/j.jterra.2014.08.003

Terzaghi, K., 1944. Theoretical soil mechanics. Chapman And Hali, Limited John Wiler And Sons, Inc, New York.

Tiwari, V.K., Pandey, K.P., Pranav, P.K., 2010. A review on traction prediction equations. J. Terramechanics 47, 191–199. https://doi.org/10.1016/j.jterra.2009.10.002

Tsytovich, N.A., 1963. Soil mechanics. Moscow: Gosstroizdat, Moscow.

Turnage, G.W., 1974. Measuring Soil Properties in Vehicle Mobility Research. Report 6. Resistance of Coarse-Grained Soils to High-Speed Penetration. Vicksburg, Mississippi.

Turnage, G.W., 1972. Tire selection and performance prediction for off-road wheeled-vehicle operations, in: Proc. 4th Int. Conf. Int. Soc. Terrain-Vehicle Systems.

Upadhyaya, S.K., Wulfsohn, D., Mehlschau, J., 1993. An instrumented device to obtain traction related parameters. J. Terramechanics 30, 1–20. https://doi.org/10.1016/0022-4898(93)90027-U

Vantsevich, V.. V., Lozynskyy, A., Demkiv, L., Klos, S., 2017. A foundation for real-time tire mobility estimation and control, in: Proceedings of the 19th International & 14th European-African Regional Conference of the ISTVS. Budapest, Hungary.

Vasil'ev, A. V., Dokychaeva, E.N., Utkin-Lubovtsov, O.L., 1969. Effect of tracked tractor design parameters on tractive performance. Moscow: Mashinostroenie, Moscow.

Wills, B., 1966. The load sinkage equation in theory and practice. Warran, Michigan.

Wong, J.-Y., Reece, A.R., 1967a. Prediction of rigid wheel performance based on the analysis of soil-wheel stresses part I. Performance of driven rigid wheels. J. o/Terramechanics 4, 81–98. https://doi.org/10.3724/SP.J.1260.2012.20007

Wong, J.-Y., Reece, A.R., 1967b. Prediction of rigid wheel performance based on the analysis of soil-wheel stresses. Part II. Towed rigid wheels. J. Terramechanics 4, 7–25. https://doi.org/10.1016/0022-4898(68)90020-7

Wong, J.Y., 2009. Terramechanics and off-road vehicle engineering: terrain behaviour, off-road vehicle performance and design, 2nd ed. Butterworth-Heinemann, Oxford.

Wong, J.Y., 2008. Theory of ground vehicles, 4th ed. John Wiley & Sons.

Wong, J.Y., 1980. Data processing methodology in the characterization of the mechanical properties of terrain. J. Terramechanics 17, 13–41. https://doi.org/10.1016/0022-4898(80)90014-2

Wong, J.Y., Garber, M., Preston-Thomas, J., 1984. Theoretical prediction and experimental substantiation of the ground pressure distribution and tractive performance of tracked vehicles. Proc. Inst. Mech. Eng. Part D Transp. Eng. 198, 265–285.

Wong, J.Y., Garber, M., Radforth, J.R., Dowell, J.T., 1979. Characterization of the mechanical properties of muskeg with special reference to vehicle mobility. J. Terramechanics 16, 163–180. https://doi.org/10.1016/0022-4898(79)90026-0

Wong, J.Y., Irwin, G.J., 1992. Measurement and characterization of the pressure-sinkage data for snow obtained using a Rammsonde. J. Terramechanics 29, 265–280. https://doi.org/10.1016/0022-4898(92)90031-E

Wong, J.Y., Preston-Thomas, J., 1983. On the characterization of the shear stress-displacement relationship of terrain. J. Terramechanics 19, 225–234. https://doi.org/10.1016/0022-4898(83)90028-9

Wong, J.Y., Radforth, J.R., Preston-Thomas, J., 1982. Some further studies on the mechanical properties of muskeg in relation to vehicle mobility. J. Terramechanics 19, 107–127. https://doi.org/10.1016/0022-4898(82)90015-5

Yoshida, K., Watanabe, T., Mizuno, N., Ishigami, G., 2006. Terramechanics-based analysis and traction control of a lunar/planetary rover. Springer Tracts Adv. Robot. 24, 225–234. https://doi.org/10.1007/10991459_22

Youssef, A.-F.A., Ali, G.A., 1982. Determination of Soil Parameters using Plate Test. J. Terramechanics 19, 129–147. https://doi.org/10.1016/0022-4898(82)90016-7